N84-32948 DRA

JAN 1984
RECEIVED
NASA STI FACILITY
ACCESS DEPT.

California Institute of Technology

Pasadena, California 91125

Science Support for the Earth Radiation Budget Sensor on the Nimbus-7 Spacecraft

Final Technical Report

for the period February 1976 - September 1982

NASA Grant Number NAS 5-22965

Andrew P. Ingersoll, Principal Investigator

Division of Geological and Planetary Sciences

California Institute of Technology

Pasadena, California 91125

Lillian Walker, Code 269, Goddard Space Flight Center, Greenbelt, MD 20771

The following publications dealing with the earth radiation budget, climate, clouds, radiation, ice sheets, and Quaternary ice ages were supported by this grant:

1. Wenkert, D.D., and A.P. Ingersoll. Empirical relations between radiative flux, cloudiness, and other meteorological parameters. Fifth Conference on Atmospheric Radiation, 31 October - 4 November, 1983, Baltimore, Maryland. Published by the American Meteorological Society, Boston, Mass.
2. Pollard, D., A.P. Ingersoll, and J.G. Lockwood. Response of a zonal climate-ice sheet model to the orbital perturbations during the Quaternary ice ages. Tellus, 32, 301-319 (1980).
3. Pollard, D., A simple parameterization for ice sheet ablation rate. Tellus, 32, 384-388 (1980).

Tellus (1980), *32*, 301–319

Response of a zonal climate–ice sheet model to the orbital perturbations during the Quaternary ice ages[1]

By DAVID POLLARD and ANDREW P. INGERSOLL, *Division of Geological and Planetary Sciences, California Institute of Technology, Pasadena, California 91125, U.S.A.*

and JOHN G. LOCKWOOD, *School of Geography, University of Leeds, Leeds LS2 9JT, England*

(Manuscript received October 24 1979; in final form January 8, 1980)

ABSTRACT

The astronomical theory of the ice ages is investigated using a simple climate model which includes the ice sheets explicitly. A one-level, zonally averaged, seasonal energy-balance equation is solved numerically for sea-level temperature T as a function of latitude and month (similar to North, 1975). Seasonally varying snow cover (which affects planetary albedo) is included diagnostically by parameterizing monthly snowfall and snowmelt in simple ways. The net annual accumulation and ablation on the ice sheet surface at each latitude are computed using the same parameterizations as for snow cover above (with T corrected for ice sheet height using a lapse rate of $-6.5\,°C\ km^{-1}$). Treatment of the ice sheets follows Weertman (1976) with ice flow approximated as perfect plasticity, which constrains the ice sheet profiles to be parabolic. The northern hemisphere's ice sheet is constrained to extend equatorward from 75°N (corresponding to the Arctic Ocean shoreline).

Model ice age curves are generated for the last several 100 Kyears by computing the seasonal climate as above once every 2 Kyears, with insolation calculated from actual Earth orbit perturbations. The change in ice sheet size for each 2 Kyear time step depends only on the net annual snow budget integrated over the whole ice sheet surface. In these model runs, the equatorward tip of the northern hemisphere's ice sheet oscillates through ~7° in latitude, correctly simulating the phases and approximate amplitude of the higher frequency components (~43 Kyear and 22 Kyear) of the deep-sea core data (Hays et al., 1976). However, the model fails to simulate the dominant glacial–interglacial cycles (~100 to 120 Kyear) of this data. The sensitivity of the model ice age curves to various parameter changes is described, but none of these changes significantly improve the fit of the model ice age curves to the data. In the concluding section we generalize about the types of mechanisms that might yield realistic glacial–interglacial cycles.

1. Introduction and summary

There is little agreement as yet on the dominant causes of the Quaternary ice ages, although many mechanisms have been suggested (described in Beckinsale, 1973; Andrews, 1975, p. 71). Data from deep-sea sediment cores provide continuous records of some climatic variables over the last several 100 Kyears (e.g., Broecker and Van Donk, 1970; Hays et al., 1976; Emiliani, 1978). These records of global ice sheet volume have been interpreted as showing quasi-periodic glacial–interglacial cycles with fast retreats from maximum to minimum volumes occurring at intervals of approximately 100 to 120 Kyears; superimposed on these cycles are secondary oscillations with smaller amplitudes and higher frequencies. Others have cautioned that some or all of the fluctuations in these records may not be periodic but essentially random (e.g., Shackleton, 1969, p. 145; Lemke, 1977). In any case, these continuous records are suitable for comparisons against any simulated records generated by quantitative models formulated to test the various suggested ice age mechanisms.

[1] Contribution number 3344 of the Division of Geological and Planetary Sciences, California Institute of Technology, Pasadena, California 91125, U.S.A.

 0040-2826/80/040301-19$02.50/0 © 1980 Munksgaard, Copenhagen

One such mechanism, the "astronomical" or "Milankovitch" theory, involves variations of incoming solar insolation due to the secular perturbations of the Earth's orbit. These variations are the only well-known external forcing of climate on ice age time scales. The historical development of the astronomical theory is lucidly described in Imbrie and Imbrie (1979). Milankovitch estimated the sensitivity of climate to this forcing using insolation-curve computations (e.g., Milankovitch, 1941), and these insolation-curves have been refined and extended by Van Woerkom (1953), Vernekar (1972), Berger (1978) and others. Other recent investigations have used seasonal climate models (Shaw and Donn, 1968; Budyko and Vasishcheva, 1971; Saltzman and Vernekar, 1971; Suarez and Held, 1976, 1979; Schneider and Thompson, 1979), explicit ice sheet models (Weertman, 1976; Birchfield and Weertman, 1978), a combined seasonal climate–ice sheet model (Pollard, 1978), and a combined annual mean climate–ice sheet–ocean model (Sergin, 1979). Also Calder (1974) and Imbrie and Imbrie (1980) have used single non-explicit "response equations". Most of these studies have generated simulated ice age curves of one sort or another, and comparisons with deep-sea core records consistently indicate that the astronomical forcing can account for the observed secondary oscillations; this positive result is consistent with the power spectrum analyses of Hays et al. (1976) and Kominz and Pisias (1979) (but see Evans and Freeland, 1977). However, none of the models above have correctly simulated the dominant glacial–interglacial cycles of the records as a response to the astronomical forcing.

This paper reports on a combined seasonal climate–ice sheet model that was described briefly in a preliminary paper (Pollard, 1978). We had hoped that the additional non-linearity due to the interactions between the ice sheets and the seasonal cycle might be the missing factor required to produce realistic glacial–interglacial cycles. With this motivation we explored the model's sensitivity to a systematic range of parameter variations. In Section 2 below, the model is formulated and its solution for the present seasonal climate is described. In Section 3, the model's long-term response to the orbital perturbations is presented, and in Section 4 we describe the sensitivity of this response to small changes in various parameter values and types of parameterizations. In the sections we emphasize some differences betwee these sensitivities and those of some other clima models, and suggest which differences in th models can account for the different sensitivitie Although our parameter changes have relativel slight effects on the fit to the present climate, son of them have significant effects on the model simulated ice age curves, i.e., on its long-ter response to the astronomical forcing. Over most c the parameter ranges these curves retain th secondary oscillations observed in the deep-se core records; however, with the model in its presen form we are still unable to generate any curve resembling the observed dominant glacial–inter glacial cycles.

Therefore, this paper supports the results of th earlier studies mentioned above. Further, since th present model still cannot account for the glacial-interglacial cycles, we suggest in Section 5 that on or more other long-term mechanisms may b important.

2. Model formulation and present-day results

The model has previously been outlined in Pollard (1978). There are two distinct parts corresponding to the two distinct time-scales of the global seasonal climate and the long-term ice sheet response. In Sections 2.1, 2.2 and 2.3 the seasonal part of the model and its solution for the present climate are described, and in Section 2.4 the ice sheets are incorporated into the model.

2.1. *Seasonal energy-balance equation*

Following North (1975), the climate through one year over a spherical globe is described by a zonally averaged, one-level energy-balance equation for sea-level air temperature T:

$$\frac{\partial}{\partial t}[CT(x,t)] - \frac{\partial}{\partial x}\left[(1-x^2)\frac{D}{R^2}\frac{\partial}{\partial x}(CT)\right] + [A + BT] = Q(x,t)(1-a) + S \qquad (1)$$

Here x is sin (latitude) and t is time. All dependent variables are defined as ~1 month running-means, so daily correlations are effectively assumed constant. Boundary conditions are $(1-x^2)^{1/2}\,\partial T/\partial x =$

0 at the poles $x = \pm 1$ (Hantel, 1972). Other symbols and their values for our "standard" model are:

$C = 4.6 \times 10^7$ J m^{-2} °C^{-1}, a constant seasonal heat capacity of the atmosphere–land–ocean system (equivalent to a layer of liquid water 11 m thick).

$D = 0.501 \times 10^6$ m^2 s^{-1}, a linear diffusion coefficient acting over the whole thickness of the layer represented by C.

$R = 6.36 \times 10^6$ m, radius of the Earth.

$A = 207$ W m^{-2}, $B = 1.9$ W m^{-2} °C^{-1}, net infrared radiation coefficients.

Q = zonal mean insolation at the top of the atmosphere, computed for any given era from the orbital elements in Berger (1976) using a solar constant of 1360 W m^{-2}.

$\boldsymbol{a} = r\boldsymbol{a}_c + (1 - r)\,\boldsymbol{a}_f$, earth-atmosphere albedo. $\boldsymbol{a}_c = 0.62$ represents areas covered by seasonal snow or ice sheet (see below), and $\boldsymbol{a}_f = 0.31 + 0.08\,[(3x^2 - 1)/2]$ represents areas free of seasonal snow and ice sheet. We set $r = 1$ north of 75 °N to represent perennial Arctic Ocean sea-ice (Ku and Broecker, 1967; Hunkins et al., 1971), and $r = 1$ south of 70 °S to represent a fixed Antarctic ice sheet (see below). At all other latitudes $r = 0.6$ when covered by seasonal snow or ice sheet, and $r = 0$ when free of seasonal snow and ice sheet.

$S = 1.27$ [J m^{-2} s^{-1}] per [g cm^{-2} month^{-1}], representing latent heat of fusion released or required at each latitude by the varying amount of seasonal snow cover (see below). The annual mean of S at each latitude is zero.

Most of these parameterizations [discussed for instance in Coakley (1979)] have found general use in many annual mean energy-balance models and are based on annual mean data. There is currently some doubt about the physical basis of the diffusive heat parameterization (Van Loon, 1979), but it may be valid for global and seasonal scales (Hartjenstein and Egger, 1979; Lorenz, 1979). The infrared radiation and albedo parameterizations are found to represent seasonal data less accurately than annual mean data, possibly due to independently varying cloud cover (White, 1976; Warren and Schneider, 1979), but we use them here for simplicity. We also neglect possible variations of cloud cover in past eras, which might be serious for the ice age problem. Unfortunately, considerable uncertainty exists for the prediction of cloud amounts even in much more complex models.

2.2. *Seasonal snowmelt and snowfall*

Seasonally varying snow cover on land at sea-level is modelled diagnostically by parameterizing monthly snowmelt and snowfall as functions of the current air temperature T and insolation Q. We use

$$\text{Snowmelt (g cm}^{-2}\text{ month}^{-1}) = \max\,[0;\, aT(°\text{C}) + bQ(\text{W m}^{-2}) + c] \tag{2}$$

Equation (2) is basically an energy-balance equation for a melting snow/ice surface with seasonal heat storage neglected, and as such is equivalent to the snowmelt parameterization of Suarez (1976). Equation (2) is also used below for the monthly ablation on ice sheet surfaces (Section 2.4). For the standard model we use $a = 10$, $b = 0.32$, $c = -47$; these values and the adequacy of this parameterization for the ice age problem are discussed in more detail in Pollard (1980).

Whereas snowmelt is a micrometeorological process, snowfall depends on synoptic-scale processes and the basic dependence of past and seasonal variations of snowfall on the zonally averaged variables T and Q is not nearly so apparent as for snowmelt. For this reason [and following Suarez (1976)] we set

$$\text{Snowfall (g cm}^{-2}\text{ month}^{-1}) = \begin{cases} P(\text{lat.}) & \text{if } T \le 0\,°\text{C} \\ 0 & \text{if } T > 0\,°\text{C} \end{cases} \tag{3}$$

where P is the present observed zonal and annual mean precipitation rate at each latitude. The northern hemispheric data given in Schutz and Gates (1971–4) is used for P(lat.) in both model hemispheres, since the present precipitation in south polar regions is clearly affected by Antarctic topography. Equation (3) is also used for the monthly accumulation on ice sheet surfaces in the standard model (Section 2.4), but some effects of ice sheet topography on the local accumulation rate will be included later.

For simplicity the model neglects variations of sea-ice. Although this might be serious for the ice age problem, seasonal and past variations of sea-ice in the northern hemisphere are somewhat smaller (by factors of ~2 to 3) than those of seasonal snow

cover and ice sheets on land (Flint, 1971, figs. 4.8, 4.9; Emiliani and Geiss, 1957, table 2; Saltzman and Vernekar, 1975, table 1).

2.3. *Fit to present climate*

As in North (1975) and North and Coakley (1979), the solution of eq. (1) is simplified by expressing the latitudinal dependences of T and the right-hand forcing in terms of the eigenfunctions of the spherical diffusion operator. Only the first three eigenfunctions are kept [i.e., Legendre polynomials 1, x, and $(3x^2 - 1)/2$], since any finer latitudinal resolution would probably not be realistic due to the coarse parameterizations used. However, the diagnostic snow budget parameterizations (2) and (3) prevent a corresponding convenient Fourier expansion in time t (cf. North and Coakley, 1979). Equation (1) is numerically integrated forward in time-steps of 1 month through consecutive years until initial transients decay to negligible levels and a repeated seasonal cycle is attained (usually after ~10 years).

Fig. 1 shows the sea-level temperature solution of the standard model, for the present orbital elements and with no northern hemispheric ice sheet. For comparison table la in Warren and Schneider (1979) shows the equivalent data for *surface* air temperature. The parameter values of the standard model given above were chosen to fit the present temperature data of the northern hemisphere. With the infrared radiation, albedo and snow budget parameterizations all fixed (somewhat arbitrarily), C was adjusted to yield realistic seasonal amplitudes at mid and high latitudes and D was adjusted to yield realistic latitudinal gradients.

The most obvious discrepancy in Fig. 1 from reality is the excessive seasonal amplitudes in the southern hemisphere due to the uniform value of C; in this respect our climate model is effectively two northern hemispheres patched together. The seasonal snow cover in the model southern hemisphere is only a crude analogy for the seasonal variation of sea-ice around Antarctica. Perhaps more seriously for the application to the Milankovitch theory, the model seasonal cycle in both hemispheres is lagged ~2 months behind the insolation cycle, which is about ~1 month more than observed in the northern hemisphere. This excessive lag has also been found by North and Coakley (1979) and Thompson and Schneider

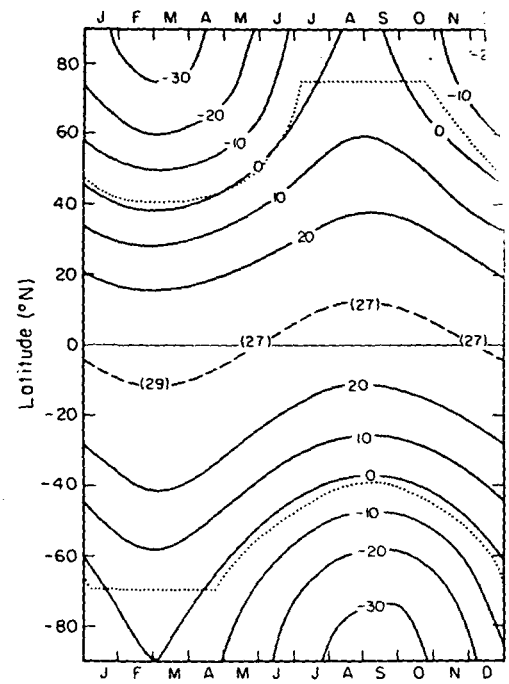

Fig. 1. Zonal mean sea-level temperature vs latitude and month for standard model present-day solution. Values shown are degrees centigrade. The dashed curve shows the latitudes of maximum temperature at each month, with maximum temperature values for some months in parentheses. The dotted curves show the latitudinal extents of seasonal snow cover in each hemisphere, for the months when snow exists equatorward of the limits of the Arctic Ocean (75°N) or Antarctic ice sheet (70°S).

(1979) in their simplest model versions, and is related to the lack of any longitudinal contrast in seasonal heat capacity between land and ocean. This excessive lag is reflected in the seasonal snow line shown in Fig. 1; the onset of snow in autumn is ~1 month later than observed (Kukla, 1975).

Fig. 2 plots the net annual "potential" snow budget for the northern hemisphere corresponding to the present-day solution. This shows the net annual snowfall minus snowmelt that would occur on any mountain glacier or ice cap surface at a given latitude and elevation h, calculated for each month from (2) and (3) but with T corrected to $T - 6.5(°\mathrm{C\ km^{-1}})\cdot h$ to allow for the atmospheric lapse rate. (Of course, snowmelt can continue below the nominal level for these surfaces so that negative net annual budgets are possible.) The zero-budget line generally agrees with present data such as the

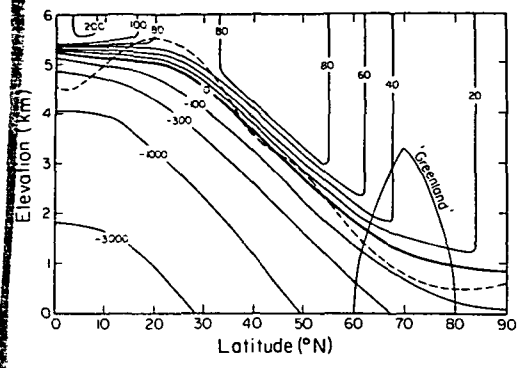

Fig. 2. Net annual snow accumulation minus ablation that would occur in the model present-day solution on hypothetical ice surfaces at given latitudes and elevations. Values shown are g cm^{-2} year^{-1}. A model ice sheet profile given by (4) roughly representing Greenland is also shown, although its contribution to the albedo a in (1) was ignored for the present-day solution. The dashed line is the observed "regional snowline" of Paschinger (1912), redrawn from Sugden and John (1975, Fig. 5.5).

generalized "regional snowline" (Paschinger, 1912), glacier altitudes in western U.S.A. (Meier, 1960), and the altitude of the equilibrium line in southern Greenland (Schuster, 1954). However, the model zero-budget line is ~500 m too high in polar latitudes north of ~70° N. There are few estimates of the present net annual budget for the entire Greenland ice sheet; approximately half of the total mass loss is by the calving of icebergs (Paterson, 1969, p. 228). The net annual accumulation minus ablation for the model Greenland profile in Fig. 2 averages to −4 g cm^{-2} over the southern half and +21 g cm^{-2} over the northern half.

2.4. *Ice sheets*

Ice sheets are incorporated into the climate model following Weertman's (1964, 1976) simple treatment. Ice sheet flow under its own weight is approximated to be perfectly plastic, which constrains the model ice sheet profiles to always remain parabolic:

$$h(s) = [\lambda(L - |s|)]^{1/2} \tag{4}$$

where h is the elevation of the ice sheet surface above sea-level, L is the half-width and s is the latitudinal distance from the ice sheet center (with s taken positive towards the equator). The ice sheet base is assumed to be isostatically depressed to depths 0.5 $h(s)$ below sea-level. λ is a constant proportional to the yield stress of ice; for our standard model we use $\lambda = 10$ m, corresponding to a yield stress of ~0.7 bars. This value is slightly less than in Weertman (1976) but still gives somewhat greater central thicknesses (by ~30%) than those modelled by Paterson (1972) and those suggested by Greenland and Antarctica today.

One model ice sheet, representing the Laurentide and Scandinavian ice sheets of past eras, is constrained to extend equatorward with its northern tip fixed at 75° N (corresponding to the Arctic Ocean shoreline). Where the margins of the real northern hemispheric ice sheets reached continental coastlines, further advance was prevented by rapid iceshelf and iceberg calving into the ocean, but their equatorial extent and overall volume were probably limited more by ablation on their southern flanks (cf. Flint, 1971, p. 484, 600). Therefore, as in Weertman (1976), the long-term variation in the model ice sheet size is controlled by the net accumulation (snowfall) minus ablation (mostly snowmelt) on its southern half only (i.e., $s > 0$). Also, since its profile is constrained by (4), any change in size is determined simply by the total ice volume added to or removed from the entire southern half. Writing the net annual accumulation minus ablation (per unit surface area) as $m(s)$, then the change in ice sheet size per unit long-term time increment $d\tau$ is given by:

$$\frac{dV}{d\tau} = \frac{d}{d\tau}[\lambda^{1/2} L^{3/2}] = \frac{1}{\rho}\int_0^L \frac{m(s)}{(1\text{ year})}\,ds \tag{5}$$

V is the volume of the southern half of the ice sheet (per unit longitudinal distance), related to L from (4). ρ is the mean ice sheet density, taken as 0.9 g cm^{-3}.

The other model ice sheet representing Antarctica is circular and centered on the South Pole. The existing Antarctic ice sheet is prevented from advancing beyond the continental bedrock by rapid calving into the southern oceans, so we do not allow this model ice sheet to ever extend equatorward beyond 70° S. In fact, the ice sheet remains at this maximum size in all ice age runs shown below, since its net annual budget is always positive. Significant ice age fluctuations in the real Antarctic ice sheet might have occurred (e.g., Wilson, 1964), but we defer this possibility to future model developments.

Model ice age curves are generated by solving (1) for one year's "climate" $T(x,t)$ once at the start

of each long-term time-step $d\tau$, using the current orbital elements. The presence of the ice sheets influences T only through the albedo a. The monthly snowmelt and snowfall at any point on the ice sheet surface is given by (2) and (3) with T corrected to $T - 6.5(°\mathrm{C\ km^{-1}}) \cdot h$ and with h given by (4). These values are integrated to give the net annual snow budget for the northern hemispheric ice sheet which is then used in (5) to determine the change in its size over the next $d\tau$ years. For all ice age curves below, we used $d\tau = 2$ Kyears. This type of procedure involving two distinct climatic time scales is described more formally in Hasselmann (1976), and has been applied to the ice age problem by Eriksson (1968) using a generalized analytical approach.

3. Ice age results: Standard model

3.1. *Ice sheet response*

The ice age simulation produced for the last 400 Kyears by our standard model is compared in Fig. 3 with a δ^{18}O deep-sea core record from Hays et al. (1976). The model curve of northern hemispheric ice sheet volume reflects the forcing of both obliquity (~41 Kyear period) and precession (~22 Kyear period), with obliquity dominating in times of small eccentricity (e.g., 60 to 0 Kyears BP). response of an ice sheet model to indivi sinusoidal forcings with these periods has described by Birchfield (1977).] The model sheet curve closely resembles an equivalent sheet curve in Weertman (1976, his fig. 6) and the response-curves in Imbrie and Imbrie (19 and coincides both in phase and approxim amplitude with the secondary oscillations of δ^{18}O record. The long-term volume inertia of ice sheets has produced a phase lag of ~5 to Kyears behind the orbital forcing (by visu comparison with various insolation-curves), co sistent with the measured phase relationships Hays et al. (1976). But despite its explicit season climate treatment, our model still lacks the dom nant glacial–interglacial cycles and the drastic ic sheet retreats (e.g., 18 to 0 Kyears BP), in commo with Weertman's and Birchfield's models.

In all ice age runs the pattern of net annual accumulation minus ablation over the ice sheets remains the same as that shown for Greenland in Fig. 2, i.e., widespread net accumulation over the central regions and much stronger net ablation over a relatively narrow strip near the equatorward tip. Therefore, the non-linear possibility suggested by Weertman (1964), of retreating ice sheets becoming

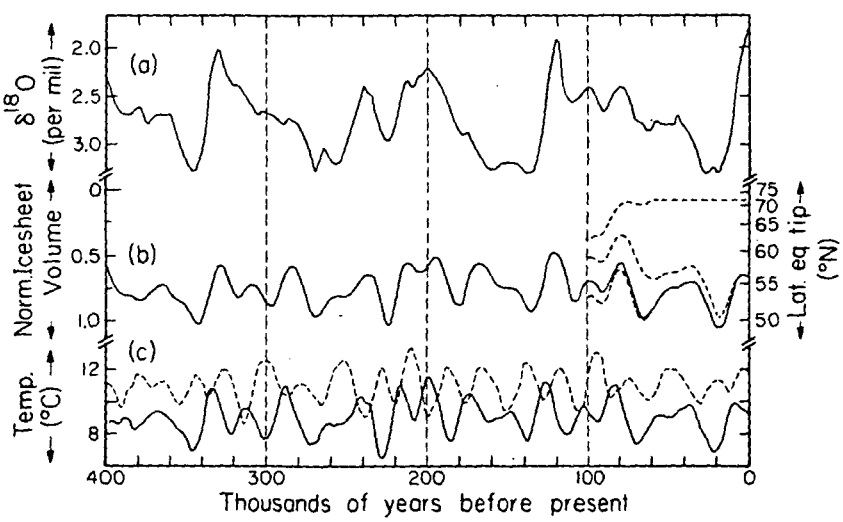

Fig. 3. (a) δ^{18}O recorded from two combined deep-sea cores (from ~45° S lat.), redrawn from Hays et al. (1976, Fig. 9). (b) Ice age curve for standard model, showing northern hemispheric ice sheet volume normalized by its volume with equatorward tip at 50° N. Right-hand scale shows corresponding latitudes of its equatorward tip. The dashed curves from 100 to 0 Kyears BP show the effect of choosing different initial ice sheet sizes at 100 Kyears BP. (c) Maximum (monthly mean) sea-level temperature at 55°N (solid curve) and 55°S (dashed curve), corresponding to the ice age run in (b).

stagnant and thus having a shorter shrinkage time-scale than growth time-scale, does not occur in any of our model runs. Imbrie and Imbrie's (1980) "response-equation" does contain such a non-linearity and produces some suggestions of glacial–interglacial cycles and drastic ice sheet retreats in response to the eccentricity variations. Consequently their fit to the $\delta^{18}O$ record is slightly better than ours, but stills leaves room for improvement.

The effect of orbital changes on the standard model can be viewed in another way in Fig. 4. Each curve shows how the northern hemispheric ice sheet would grow or recede as a function of its size, for various combinations of the orbital elements. This figure is a development of fig. 7 in Weertman (1961), who analyzed the general shape of the curves as a simple geometrical consequence of ice sheet topography and the typical net snow budget pattern. As expected (Berger, 1978), the grouping of the curves in Fig. 4 shows that eccentricity plus precession are most important for large (low latitude) ice sheets, whereas obliquity has an important effect for small (high latitude) ice sheets. For fixed orbital elements, the ice sheet size would move along the relevant curve until it either arrives at a stable point S or is ablated away to the Arctic shoreline. The ice sheet tip in the ice age run of Fig. 3 (b) varies between ~50° N and ~60° N, and this is the region in Fig. 4 where approximately half of the orbital combinations are enlarging the ice sheet towards stable points S and the other half are ablating it toward the Arctic shoreline. However, this potential amplitude of some 30° in latitude implied by Fig. 4 is reduced to ~10° latitude in Fig. 3 (b) by the volume inertia of the ice sheet.

The full amplitude of ~30° in latitude is reflected in the dashed curves in Fig. 3 (b), which show the effect of choosing different initial ice sheet sizes at 100 Kyears BP. If the initial tip position is north of ~61° N, the ice sheet does not return to the solid curve. Instead it is ablated back to the Arctic shoreline and remains there forever, since the majority of orbital combinations produce negative regimes for these small ice sheet sizes. This is an example of an "intransitive" climate system (Lorenz, 1970), with two possible stable branches depending on the initial conditions. The orbital forcing by itself is insufficient to produce transitions from one branch to another, and so we effectively had to "choose" the ice-sheet-free branch for the present-day fit in Section 2.3, and the other branch exhibiting ice sheet oscillations for this section. Some modifications described below will make these transitions possible (Fig. 10) or will eliminate the distinction between the two branches (Fig. 8).

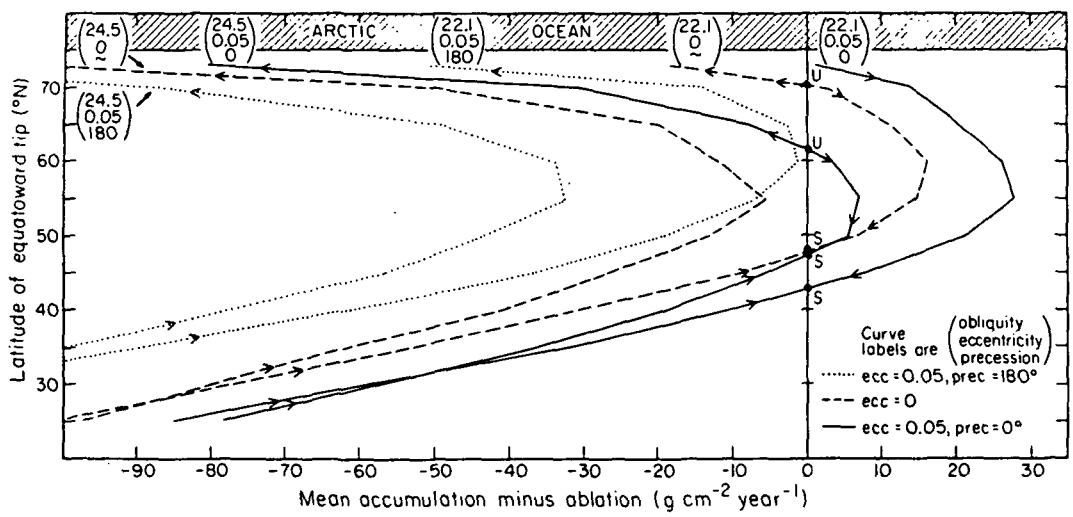

Fig. 4. Curves of net annual northern hemispheric ice sheet budget (averaged over southern half) as functions of its size, for various combinations of the orbital elements. (Precession is defined here so that it is zero when the northern hemispheric winter solstice coincides with perihelion, and 180° when this solstice coincides with aphelion.) These curves are for the standard model. For fixed orbital elements, "S" are stable equilibrium points, "U" are unstable equilibrium points, and the arrows show directions of ice sheet growth and decay.

The time-scale on which the dashed curves in Fig. 3 (b) converge onto one branch or another is on the order of ~40 Kyears. This represents the intrinsic time-scale of the quasi-linear ice sheet response on either branch, and is roughly consistent with the amount of lag (mentioned above) of the solid curve in Fig. 3 (b) behind the orbital forcing. Because the model has only one long-term time-derivative [in (5)], there can be no free internal oscillations of the system in the absence of external forcing, as there are in Sergin's (1979) climate–ocean–ice sheet model.

3.2. *Temperature response*

Fig. 3 (c) shows the variation of maximum summer temperature at particular latitudes for the standard ice age run. The temperature curve for 55° N seems (visually) to lag only ~0 to 4 Kyears behind the orbital forcing, considerably less than the ice sheet volume curve. This summer temperature curve has roughly the same phase as various northern hemispheric curves in Shaw and Donn (1968), Suarez and Held (1979) and Schneider and Thompson (1979). The higher-frequency component of the temperature curve for 55° S reflects the forcing of precession, which is 180° out of phase between the two hemispheres. The phase of the 55° S curve does not agree with that of the secondary oscillations of the "*Ts*" deep-sea core record for ~45° S in Hays et al. (1976); the latter is found to lead those of the $\delta^{18}O$ core record by ~2 Kyears. This disagreement may be due to th shortcomings in the model formulation for th southern hemisphere. [Both Suarez and Held (1979) and Schneider and Thompson's (1979 models have realistic southern hemispheric seasonal heat capacities, but they appear to yield southern hemispheric temperature phases that are opposite to each other.]

Table 1 summarizes the sensitivity of northern hemispheric temperatures to some particular changes in the orbit and ice sheet size (analogous to Fig. 4). The most extreme orbital variation with no northern hemispheric ice sheet (col. 4, Table 1) causes seasonal temperature changes comparable to those caused through the albedo a by a full glacial–interglacial ice sheet variation at fixed orbit (col. 5, Table 1). However this ice sheet variation causes annual mean temperature changes at mid and high latitudes that are considerably larger than those caused by the orbital variations, in agreement with the trend in Sergin (1979, fig. 16).

We now compare the sensitivities in Table 1 to those of other models. The sensitivities of annual mean temperatures to the orbital variations (cols. 2 to 4, Table 1) are similar to those of Schneider and Thompson's (1979) model, but are generally less than 1/4 of those in Suarez and Held (1979). The extra sensitivity in the latter model is probably due to greater albedo feedback of seasonal snow. As discussed by Suarez and Held, albedo feedback is greater for models like theirs having realistic land–ocean longitudinal contrast. However in

Table 1. *Differences of sea-level temperatures at particular latitudes between different orbits (as defined in Fig. 4) with no northern hemispheric ice sheet (columns 2 to 4), and between different ice sheet sizes with the same orbit (column 5)*

Latitude	δ orbit $\begin{pmatrix}24.5\\0\\\sim\end{pmatrix}-\begin{pmatrix}22.1\\0\\\sim\end{pmatrix}$	δ orbit $\begin{pmatrix}22.1\\0.05\\180\end{pmatrix}-\begin{pmatrix}22.1\\0.05\\0\end{pmatrix}$	δ orbit $\begin{pmatrix}24.5\\0.05\\180\end{pmatrix}-\begin{pmatrix}22.1\\0.05\\0\end{pmatrix}$	δ ice sheet tip (73° N–50° N)
89° N	$\begin{pmatrix}3.4\\-0.7\end{pmatrix}$ 1.1	$\begin{pmatrix}2.5\\-2.4\end{pmatrix}$ −0.4	$\begin{pmatrix}5.8\\-3.1\end{pmatrix}$ 0.7	$\begin{pmatrix}6.1\\2.5\end{pmatrix}$ 4.0
45° N	$\begin{pmatrix}1.6\\-1.1\end{pmatrix}$ 0.1	$\begin{pmatrix}4.5\\-4.1\end{pmatrix}$ −0.3	$\begin{pmatrix}6.1\\-5.1\end{pmatrix}$ −0.1	$\begin{pmatrix}3.8\\2.1\end{pmatrix}$ 2.6
1° N	$\begin{pmatrix}-0.9\\-0.7\end{pmatrix}$ −0.7	$\begin{pmatrix}6.0\\-5.9\end{pmatrix}$ 0.0	$\begin{pmatrix}5.2\\-6.6\end{pmatrix}$ −0.7	$\begin{pmatrix}0.4\\0.7\end{pmatrix}$ 0.6

The values in parentheses are differences in °C for the months of maximum northern hemispheric summer temperatures (upper value) and minimum northern hemispheric winter temperatures (lower value). The other value outside the parentheses is the annual mean temperature difference in °C.

sagreement may be due to the the model formulation for the here. [Both Suarez and Held's neider and Thompson's (1979) realistic southern hemispheric acities, but they appear to yield eric temperature phases that are ther.]

arizes the sensitivity of northern peratures to some particular it and ice sheet size (analogous to extreme orbital variation with no eric ice sheet (col. 4, Table 1) emperature changes comparable through the albedo a by a full l ice sheet variation at fixed orbit However this ice sheet variation ean temperature changes at mid that are considerably larger than the orbital variations, in agree- nd in Sergin (1979, fig. 16).

are the sensitivities in Table 1 to odels. The sensitivities of annual es to the orbital variations (cols. 2 similar to those of Schneider and 9) model, but are generally less in Suarez and Held (1979). The n the latter model is probably due feedback of seasonal snow. As rez and Held, albedo feedback is nels like theirs having realistic itudinal contrast. However in

etween different orbits (as defined between different ice sheet sizes

2.1 .05)	δ ice sheet tip (73° N–50° N)
7	$\binom{6.1}{2.5}$ 4.0
1	$\binom{3.8}{2.1}$ 2.6
7	$\binom{0.4}{0.7}$ 0.6

num northern hemispheric summer tures (lower value). The other value

addition to this effect, Suarez and Held have adjusted their parameter values so that over nearly the whole range of orbital variations, their northern hemispheric minimum summer snowline remains equatorward of the Arctic Ocean; in contrast, our model solutions (for cols. 2 to 4, Table 1) have no seasonal snow (i.e., no albedo feedback) in summer equatorward of our Arctic Ocean shoreline at 75° N, as in Fig. 1. The real summer snowline seems to be roughly intermediate between these two model situations (Dickson and Posey, 1967; Kukla, 1975; Williams, 1978).

The reductions of T in summer due to the ice sheets (col. 5, Table 1) are comparable to those found by CLIMAP (1976) data for sea-surface temperatures of the last glacial maximum. The corresponding air temperature reductions found by the more complex zonal model of Saltzman and Vernekar (1975) and the GCM of Gates (1976a,b) are generally larger than in col. 5 (by ~100%), whereas the GCM of Williams (1974) has found much larger air temperature reductions (of $\gtrsim 20$ °C).

These differences in the temperature sensitivities of the various models lead to some uncertainty in applications to the Milankovitch theory. For instance, it may be that if we replaced our simple climate model with Suarez and Held's model, the amplitude of the ice sheet response in Fig. 3 (b) (as well as the annual mean temperature response) would be increased by a factor of ~4. However, our simple model already realistically simulates the secondary oscillations of the $\delta^{18}O$ data, and any large alteration of its ice sheet sensitivity would destroy this agreement. What *is* needed is a model modification to produce the dominant glacial–interglacial cycles of the data.

4. Ice age results: parameter sensitivity

The aim of this section is to explore the range of parameter values and parameterizations that still yield realistic ice age secondary oscillations, and also to search for a model modification that may produce the full glacial–interglacial cycles. We do not concentrate on the sensitivity of particular *climate* solutions $T(x,t)$ *per se*. Most of the parameter changes examined below do slightly perturb the present-day solution of Section 2.3 (e.g., by $\lesssim \pm 2$ °C in Fig. 1, by $\lesssim \pm 500$ m in the zero-budget line altitude in Fig. 2), but these perturbations are minor compared to the existing coarseness of the fit to present data.

4.1. *Climate parameter variations*

Fig. 5 shows the sensitivity of the ice age curve to small variations in the diffusion parameter D, with all other parameters held constant. Only the response for the last 100 Kyears is shown, but this is sufficient to demonstrate the behavior for any time period. We have performed the same exercise for small variations (~2 to 10%) in each one of the "climate parameters" C, B, a_f, a_c, a, b, and c [appearing in (1) and (2)] in turn, all with virtually the same result as in Fig. 5.

For parameter changes that have the effect of reducing the summer temperatures in mid and high latitudes or reducing ablation for a given temperature and insolation, the mean position of the ice age curves move smoothly equatorward. The effect of precession (~22 Kyear period) becomes more pronounced equatorward of ~45° N, as might be expected from Fig. 4. Apart from this effect, the basic model response is unchanged and still resembles the secondary oscillations of the ice age data. [For larger parameter variations than shown here, a sudden transition to ice-sheet-covered northern hemispheric continents might be expected. In other runs (not shown) investigating solar constant variations, ice sheets could exist in stable equilibrium down to ~20° N for solar constant reductions of up to ~5%, beyond which they grew down to the equator.] For parameter changes in the other direction, there is a sudden transition to an ice-sheet-free northern hemisphere; there is no stable mean ice sheet tip position between ~55° N and the Arctic shoreline. Once the minimum size is reached, the ice sheet never grows out again [as in Fig. 3 (b)].

The behavior in Fig. 5 can be explained by referring to Fig. 4. Climate parameter variations basically have the effect of shifting the pattern of curves in Fig. 4 horizontally relative to the "regime" x-axis. For small shifts toward more negative regimes, ice sheet sizes in the range ~50° to 60° N begin to lie more on the unstable ablating branches of most orbital curves, and so are reduced back to the Arctic shoreline. For relatively large shifts toward more positive regimes, more orbital curves have stable points S and the range of latitudes of these stable points smoothly moves equatorward.

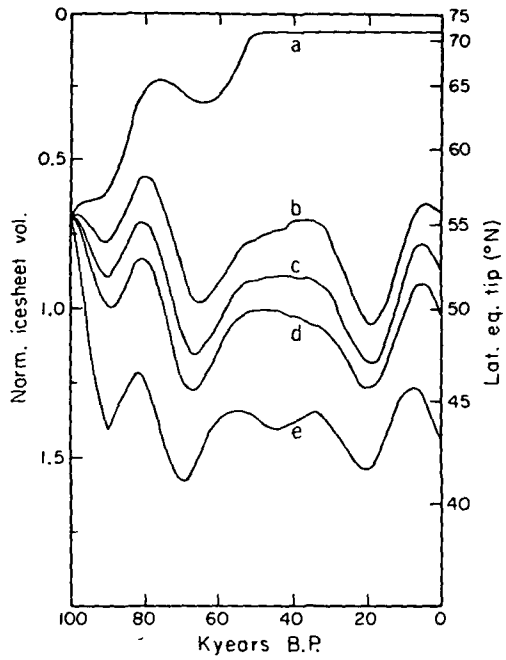

Fig. 5. Ice age curves for the standard model except: (a) Diffusion coefficient $D = (0.31/0.30) \times$ standard model value. (b) Diffusion coefficient $D = (1) \times$ standard model value. (c) Diffusion coefficient $D = (0.29/0.30) \times$ standard model value. (d) Diffusion coefficient $D = (0.28/0.30) \times$ standard model value. (e) Diffusion coefficient $D = (0.23/0.30) \times$ standard model value.

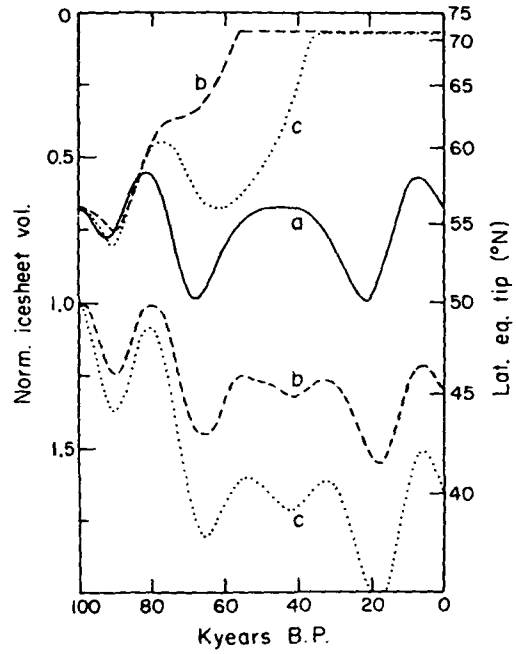

Fig. 6. Ice age curves for the standard model except: (a) Solid curve: Diffusion coefficient $D = (0.23/0.30) \times$ standard model value, and $a_f = a_f^{(s)} + 0.017$, $a_c = a_c^{(s)} - 0.14$, where $a_f^{(s)}$ and $a_c^{(s)}$ are the standard model albedos for snow–ice/free and snow–ice/covered surfaces respectively. (b) Dashed curves: Diffusion coefficient $D = (0.37/0.30) \times$ standard model value, and $a_f = a_f^{(s)} - 0.015$, $a_c = a_c^{(s)} + 0.134$, showing two different choices of initial ice sheet size. (c) Dotted curves: Seasonal heat capacity $C = (7/11) \times$ standard model value, and with ablation rates (2) reduced by a factor 0.42, showing two different choices of initial ice sheet size.

If only one climate parameter is varied at a time, the range of interest is limited by the sudden retreat of the ice sheets [as in Fig. 5 (a)]. Another common sensitivity test (Coakley, 1979; Warren and Schneider, 1979) is to vary two or more parameters simultaneously so that their basic effects partially cancel each other and the mean ice sheet position can be held "on scale". Three examples of this are shown in Fig. 6. In curves (a) and (b) large variations in D are compensated by changes in the albedo contrast to maintain nearly the same temperature field for a given orbit and ice sheet size. In curves (c) a low value of the seasonal heat capacity C (which produces larger seasonal cycles and higher summer temperatures at high latitudes) is compensated crudely by reducing the ablation rate by a constant factor.

For the large value of D and the low value of C, two different initial ice sheet sizes are chosen to show that the lower branch of stable ice sheet tip positions has shifted south to ~40° to 45° N latitude. This is because both these parameter variations favor the net snow budget of large ice sheets relative to small ones, due to increased ice sheet albedo feedback for large D and due to larger summer temperature increases at higher latitudes for low C. Consequently the stable points "S" in the corresponding orbital-curve diagrams (not shown) are located ~10° to 15° further south than in Fig. 4. This is the only real difference in Fig. 6 from the standard model response, and the amplitude and phase of the ice sheet oscillations have remained basically the same.

We have not repeated the exercise in Fig. 6 for

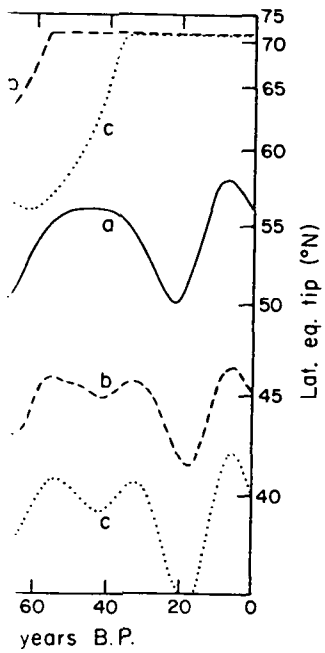

es for the standard model except: sion coefficient $D = (0.23/0.30) \times$ e, and $a_f = a_f^{(s)} + 0.017$, $a_c =$ $^{(s)}$ and $a_c^{(s)}$ are the standard model free and snow–ice/covered surfaces hed curves: Diffusion coefficient D ndard model value, and $a_f = a_f^{(s)}$ .134, showing two different choices ize. (c) Dotted curves: Seasonal /11) × standard model value, and (2) reduced by a factor 0.42, choices of initial ice sheet size.

ie of D and the low value of C, ice sheet sizes are chosen to branch of stable ice sheet tip ed south to ~40° to 45°N ecause both these parameter net snow budget of large ice nall ones, due to increased ice k for large D and due to larger e increases at higher latitudes ently the stable points "S" in orbital-curve diagrams (not 10° to 15° further south than only real difference in Fig. 6 odel response, and the ampli- he ice sheet oscillations have e same.

ted the exercise in Fig. 6 for

all possible combinations of parameter variations [of which there are on the order of 10^5, as noted by Imbrie and Imbrie (1980)]. In the development of this model we experimented relatively unsystematically with many (perhaps ~200) combinations of parameter values that appear in eqs. (1) to (5), and never found any types of ice age response other than those described in this paper.

The constants in the ablation parameterization (2) are not tightly constrained by present glacial data (Pollard, 1980). We ran several ice age curves (not shown) using widely different values; for instance $(a,b,c) = (20,0,80)$ respectively so that ablation depended only on temperature, and $(a,b,c) = (5,0.32,-68)$ so that the temperature dependence was half that of the standard model. In these runs, the responses to the orbital perturbations were basically unchanged from the standard model, producing secondary oscillations of the same phase and magnitude without any suggestion of full glacial–interglacial cycles. [The temperature dependence in (2) cannot be eliminated completely. With $a = 0$, the model yields unrealistic seasonal cycles with snow-free high latitudes in summer and perennial snow in mid-latitudes, due to the latitudinal forms of the precipitation rate and the seasonal insolation forcing. In the present model, ablation and seasonal snow cover must be controlled mainly by temperature.]

Henderson-Sellers and Meadows (1979) and Cogley (1979) have suggested that variations of high-latitude ice cover have affected the planetary albedo to a much lesser degree than in many other models. Correspondingly Fig. 7 (a) shows a run with no albedo feedback at all, neither from the seasonal snow nor from the ice sheets; a is simply a constant function of latitude. The present-day solution with this parameterization still fits the present data as well as the standard model in Section 2.3. The ice age response in Fig. 7 (a) is basically unchanged from that of the standard model, suggesting that ice-albedo feedback is not a significant mechanism for the secondary oscillations of the ice age records. Fig. 7 (b) shows another run using an albedo partly dependent on solar zenith angle, as investigated by Lian and Cess (1977). Again there was no basic change in the ice age response, as might be expected from the indifference of Fig. 7 (a) to the albedo parameterization.

Fig. 7 (c) shows an ice age run for an annual

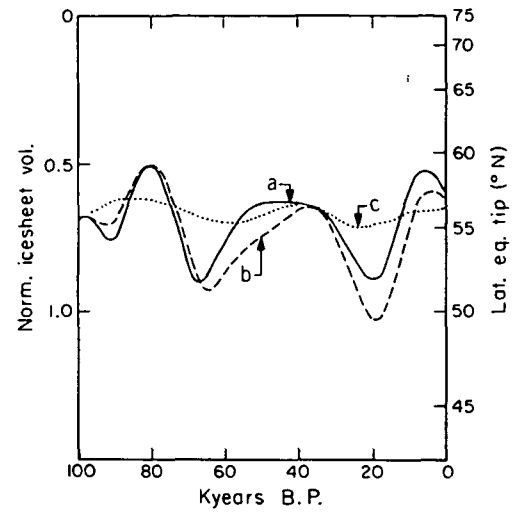

Fig. 7. Ice age curves for the standard model except: (a) Solid curve: Using fixed albedos. $a = 0.35 + 0.2[(3x^2 - 1)/2]$ always. (b) Dashed curve: Using fraction of hourly insolation absorbed by the earth-atmosphere system $= f[0.35 \cos(s) + 0.479]$, where s is hourly solar zenith angle and $f = 1$ or 0.6 for snow/ice-free or snow/ice-covered surfaces respectively. (c) Dotted curve: Using annual mean insolation in eq. (1), and using $(a,b,c) = (10,0,122)$ respectively in eq. (2). Also setting $S = 0$ in eq. (1).

mean version of our model. For this version, the current annual mean insolation at each latitude is used for Q in (1), and ablation depends only on T. The resulting annual mean climate solutions for individual years are much the same as in North (1975), with a sea-level snowline potentially at ~70°N (except that for Fig. 7 (b), this latitude region is occupied by ice sheet). The peak-to-peak amplitude of the ice sheet tip response of the annual mean version is reduced to ~1.5° in latitude, and temperature variations at fixed latitudes are all $\lesssim 1$ °C. Therefore we find that the seasonal cycle is necessary for our model to produce realistic secondary oscillations. We have seen that seasonal albedo feedback is not necessary for the seasonal model's ice age response [Fig. 7 (a)], so seasonal albedo feedback cannot be the important difference between the seasonal and annual mean models. The important difference seems to be due to the fact that the orbital perturbations change the seasonal cycles of temperature (at the latitudes around the ice sheet tip) much more than the annual mean temperatures. The ice sheets respond just as much

to changes in the seasonal cycles as to the annual mean changes, due mostly to the non-linearity in the ablation parameterization (2), and so the seasonal version of the model produces a much larger ice sheet response.

We now compare the sensitivities in Fig. 7 to those of two other seasonal energy-balance models. North and Coakley's (1979) model has a seasonal snowline, a perennial "ice line" fixed to the −10°C zonal and annual mean isotherm, and also contains longitudinal land–ocean asymmetry. In response to obliquity changes of 1.2°, their perennial ice line changes by 3° in latitude for the seasonal version and 2° in latitude for the annual mean version. Presumably for obliquity variations of 2.4° (more representative of the actual orbital perturbations) this would imply ice line changes of 6° lat. (seasonal version) and 4° lat. (annual mean version). In contrast, our model ice sheet tip varies by 7° lat. (seasonal version) and ~1.5° lat. (annual mean version) in response to the actual orbital perturbations (including precession). This points to an important difference between the two models: their ice line responds only to the mean annual temperature and so the increased response of their seasonal version is due to slight variations in the residual correlation between the seasonal cycles of albedo and insolation. However, as discussed above, our more non-linear ice sheets respond directly to variations in the seasonal cycles themselves, resulting in a greater difference in response between seasonal and annual mean versions.

Schneider and Thompson (1979) find that the sensitivity of temperature to the orbital perturbations in their seasonal climate model is decreased by ~30% by using fixed (constant) albedos compared to using seasonally varying albedos. When our model is run with no ice sheets we find basically the same result as theirs, and the different result implied by Fig. 7 (a) is due to the presence of the ice sheets. The albedos in our standard model can change only in the winter months when the seasonal snowline extends equatorward beyond the ice sheet tip; during the summer months the ice sheets prevent any change in albedo and so the seasonal variation of albedo is reduced considerably (cf. discussion of Table 1).

North and Coakley (1979) and Thompson and Schneider (1979) both find that the sensitivities of their models to 1% solar constant variations are nearly the same for seasonal and annual mean versions, which at first sight contradicts the r in Fig. 7 (c). However, solar constant variat primarily affect the annual mean insolation and the seasonal cycles, and so are a fundament different type of forcing from the orbital per bations in Fig. 7. [In fact we do find (not sho that the sensitivities to small solar consi variations of our seasonal and annual m versions are very nearly the same, with glo annual mean temperatures changing by 1.8 °C 1% change in solar constant.]

We now mention two other modifications to model that were tried. In some runs, monthly zo precipitation was parameterized as a function sea-level temperature T and $\partial T/\partial$latitude, opposed to the fixed precipitation of the standa model. Several similar functions were tried, f instance

$$\text{Precip. (g cm}^{-2}\text{ month}^{-1}) = \max\,[4;|10\,\partial T(^\circ\text{C})/\partial\,\text{lat. (deg.)}|]\;\exp[T(^\circ\text{C})/17]$$

This is a very rough fit to present seasonal zona data in Schutz and Gates (1971–4); simila parameterizations have been investigated b Schneider and Thompson (1977). The functio implies a reduction in precipitation during glacia maxima associated with lower saturation vapo pressures, which has sometimes been suggested a a significant ice age factor. However, these para meterizations produced no ice age curves signifi cantly different from those of the standard model suggesting that the secondary oscillations of the ic sheet records have been caused more by ablatio variations than accumulation variations. Data i Yapp and Epstein (1979) and Ruddiman an McIntyre (1979) are suggestive of important ic age precipitation variations due to changing longitudinal land–ocean temperature contrasts, bu this is outside the scope of the present model.

In several runs (not shown) we crudely at tempted to simulate the long-term effect of th short-term "random" weather variability, a analyzed by Hasselmann (1976) and Lemk (1977). In these runs a random term, rectangularl distributed between ±10 g cm^{-2} year^{-1} [i.e., ±2 × 10^4 g cm^{-2} (2 Kyear)$^{-1}$], was added to the mea ice sheet budget at each 2 Kyear time step. Th resulting ice sheet volume curves were not signifi cantly different from the standard model response with no suggestion of any drastic ice sheet retreats.

hich at first sight contradicts the result c). However, solar constant variations ffect the annual mean insolation and not l cycles, and so are a fundamentally pe of forcing from the orbital pertur- ig. 7. [In fact we do find (not shown) ensitivities to small solar constant of our seasonal and annual mean very nearly the same, with global temperatures changing by 1.8 °C per n solar constant.]

nention two other modifications to the ere tried. In some runs, monthly zonal was parameterized as a function of nperature T and $\partial T/\partial$latitude, as he fixed precipitation of the standard ral similar functions were tried, for

$^{-2}$ month^{-1})

10 ∂T(°C)/∂ lat. (deg.)]

(°C)/17]

y rough fit to present seasonal zonal utz and Gates (1971–4); similar ions have been investigated by d Thompson (1977). The function ction in precipitation during glacial iated with lower saturation vapor ch has sometimes been suggested as e age factor. However, these para- produced no ice age curves signifi- from those of the standard model, the secondary oscillations of the ice have been caused more by ablation accumulation variations. Data in stein (1979) and Ruddiman and 9) are suggestive of important ice on variations due to changing d–ocean temperature contrasts, but e scope of the present model.

uns (not shown) we crudely at- ulate the long-term effect of the ndom" weather variability, as Hasselmann (1976) and Lemke runs a random term, rectangularly een ±10 g cm^{-2} year^{-1} [i.e., ±2 × year)$^{-1}$], was added to the mean at each 2 Kyear time step. The t volume curves were not signifi- om the standard model response, n of any drastic ice sheet retreats.

4.2. *Ice sheet parameter variations*

No really different ice age responses in either the amplitude or the phase of the secondary oscillations have been produced by the climate parameter variations above. As shown below, parameter variations concerning the ice sheet can have somewhat greater effects.

Fig. 8 show ice age runs with the precipitation on all ice sheet surfaces reduced by a factor exp [$-h$(km)/3] from the zonal mean, where h is the local ice sheet elevation given by (4). To balance this, ablation is also reduced slightly. This crudely models the topographic blocking of storms carrying precipitation to the ice sheet interiors, as observed on Antarctica and Greenland today (Mock, 1967; Chorlton and Lister, 1968). The effect of slight variations in the weather parameters in Fig. 8 is similar to Fig. 5, but now there is no sudden transition to an ice-sheet-free northern hemisphere, and stable mean ice sheet tip positions can exist between ~55° N and the Arctic shoreline. The corresponding orbital-curve diagram is shown in Fig. 9; these curves do not bend back to negative regimes for small ice sheets nearly so much as in Fig. 4, allowing small stable ice sheets. This also implies that ice age runs with different initial ice sheet sizes converge to the same curve, as shown by the dashed curve in Fig. 8; the equivalent curve in Fig. 3 (b) retreated to the Arctic shoreline.

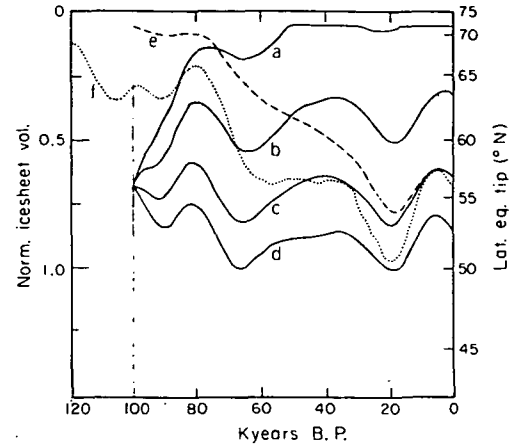

Fig. 8. Ice age curves for the standard model except that precipitation on ice sheets is reduced by factor exp [$-h$(km)/3] from the zonal mean, and: (a) Ablation coefficient b = 0.30 in eq. (2). (b) Ablation coefficient b = 0.28 in eq. (2). (c) Ablation coefficient b = 0.26 in eq. (2). (d) Ablation coefficient b = 0.24 in eq. (2). (e) Dashed curve is as for curve (c) but with different initial ice sheet size. (f) Dotted curve is for standard model except that precipitation on ice sheets is altered by factor 2 exp [$-h$(km)/3] from the zonal mean.

The change from Fig. 4 to Fig. 9 can be explained as follows: the reduction in precipitation is greater for large ice sheets than for small ones, whereas the ablation reduction we have used to

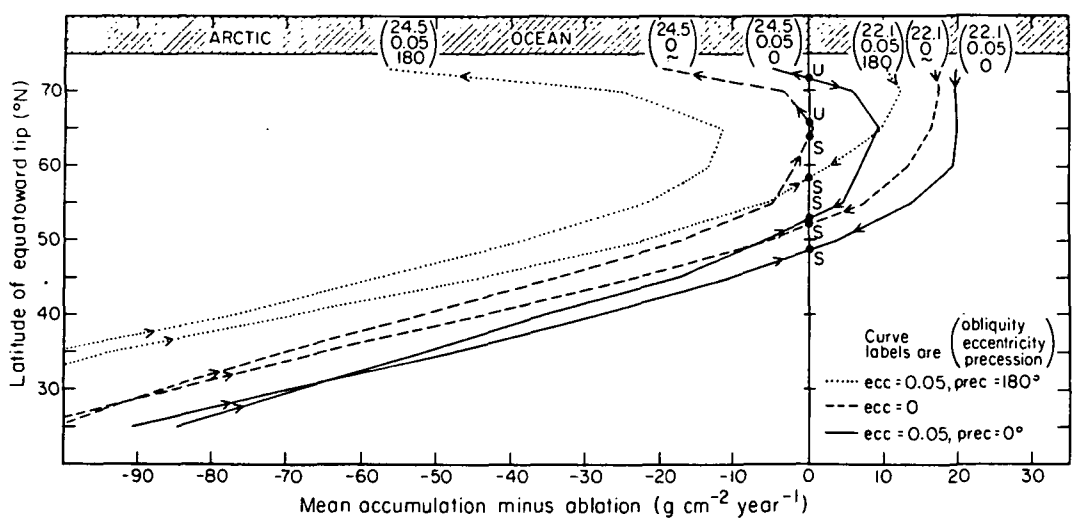

Fig. 9. As Fig. 4 except that precipitation on ice sheets is reduced by factor exp [$-h$(km)/3] from the zonal mean, and b = 0.26 in eq. (2).

balance these reductions affects all ice sheet sizes equally. Any equivalent modification to the model, that favors the net snow budget of small ice sheets relative to large ice sheets, produces changes in the same direction as Fig. 9; for instance, smaller lapse rate magnitudes than 16.51 °C km^{-1} in (2), thinner ice sheet profiles, or less ice sheet albedo feedback. (The trend in the opposite direction was described briefly in connection with Fig. 6.)

In contrast to the precipitation reductions in ice sheet interiors, the steep flanks of ice sheets can locally increase precipitation on the sides facing the prevailing winds (Mock, 1967). To crudely test this effect we ran some ice age curves (not shown) with precipitation on all ice sheet surfaces increased by a factor of 2 over the zonal mean (and with ablation similarly increased by a constant factor). However, the only effect on the response was the predictable one of doubling the peak-to-peak amplitude of the secondary oscillations to ~15° in latitude. There were still no suggestions of a realistic glacial–interglacial cycle.

The amplitude of the response can also be increased by using thinner ice sheets, i.e. by reducing the value of λ in eq. (3) below 10 meters. Fig. 10 shows two runs using $\lambda \approx 4$ meters, which lies slightly below the range of values appropriate for existing ice bodies (Paterson, 1972, table 2). Perhaps more unrealistically, isostatic depression of the land surface beneath the ice sheet is ignored. These curves show transitions between a mean ice sheet position around ~55° N (from 300 to 200 and from 100 to 0 Kyears BP), and a much smaller mean position trapped near the Arctic shoreline (from 200 to 100 Kyears BP). This type of response is intermediate between those in Figs. 5 and 8; now the increased amplitude of the basic oscillations (forced by obliquity and precession) is sufficient to ocassionally bridge the gap between the two stable positions. This new situation might be classified as "almost intransitive" (Lorenz, 1970).

We have chosen slightly different minimum ice sheet sizes for the two curves in Fig. 10, and this difference can occasionally be important in allowing an "escape" from the Arctic shoreline or not (e.g., at ~150 Kyears BP). In reality regional land topography becomes important for these nascent ice sheets (Loewe, 1971; Barry et al., 1975), and the present model just suggests that such details for small ice sheets can sometimes affect the form of the subsequent response.

The curves in Fig. 10 are notably similar to many of the curves produced by the ice sheet models of Weertman (1976) and Birchfield and Weertman (1978), and also to the curve produced by Calder's (1974) response equation. The ice sheet thicknesses used by Birchfield and Weertman ($\lambda =$ 14 meters) are more similar to our standard model value, and considerably greater than those in Fig. 10. Presumably this is compensated by our climate model producing smaller net snow budget variations (due to the orbital forcing) than those produced by their more geometrical parameterization; the curve in Weertman (1976), Fig. 6) that is most similar to our standard model curve [Fig. 3 (b)] uses accumulation and ablation values that are generally ~1/2 to ~1/3 of those in our model. As in their studies, we have also tried using circular

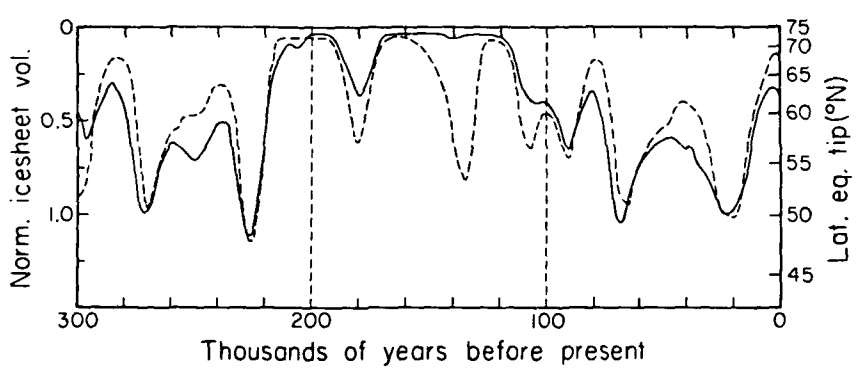

Fig. 10. Ice age curves for standard model except with no isostatic depression below the ice sheets, and: (a) Solid curve: $\lambda = 4.2$ meters in eq. (3), and values of (a,b,c) in eq. (2) are (8, 0.234, −39.2) respectively. Also minimum ice sheet half-width = 1.5° lat. (b) Dashed curve: $\lambda = 3.6$ meters in eq. (3), and values of (a,b,c) in eq. (2) are (8, 0.226, −39.2) respectively. Minimum ice sheet half-width = 2.0° lat.

rather than linear northern hemispheric ice sheets, and have taken the ice sheet budget over the whole surface and not just the southern half. However these modifications leave our ice age runs basically unchanged. Although their curves and those in Fig. 10 might be considered suggestive of possible longer-period cycles and their spectra may contain some power at periods $\gtrsim 100$ Kyears (Birchfield and Weertman, 1978), the models still fail to produce realistic glacial–interglacial cycles. In fact, the "secondary" oscillations in Fig. 10 are much larger than those observed in the records.

5. Concluding section

In the various ice age runs above, the amplitudes of the northern hemispheric ice sheet volume fluctuations are generally between 20% to 50% of the maximum glacial volume, corresponding to between ~4° and 10° in the latitude of its equatorward tip. These fluctuations generally agree both in phase and amplitude with the secondary oscillations of $\delta^{18}O$ deep-sea core records, at least to within the small variations from record to record and within the mixed effects of ice sheet volume and ocean temperature in the $\delta^{18}O$ signal (Emiliani and Shackleton, 1974).

The components of the model that are necessary to produce this response are the explicit treatment of ice sheet topography and snow budget, and the seasonal and latitudinal variations of temperature. In fact, given these features we cannot find any reasonable parameter changes that do *not* give realistic secondary oscillations (except for cases giving an ice-sheet-free northern hemisphere). Using annual mean insolation in (1) reduces the ice age response by a factor of ~4, but eliminating albedo feedback has very little effect on the model's response (see Fig. 7). However, albedo feedback of the ice sheets might still be important for full glacial–interglacial cycles. These sensitivities are related to the ice sheet and ablation parameterizations, as discussed in connection with Fig. 7.

We have not been able to produce realistic glacial–interglacial cycles with the present model. Starting at small ice sheet size, the model can plausibly simulate the relatively slow ~80 Kyear growths to glacial maximum [for instance by adjusting the ice sheet precipitation parameterization as in Fig. 8 (f)]; it is the drastic ~20 Kyear retreats back to interglacials that the model lacks. The estimates of Laurentide ice sheet volumes in Paterson (1972) imply mean ice sheet budgets averaging ~ -50 g cm^{-2} yr^{-1} between 14 and 9 Kyears BP. (Ice sheet retreat after this point was probably accelerated strongly due to being split by marine waters of Hudson Bay at ~8 Kyears BP.) In our model ice age runs the mean northern ice sheet budget varies only between $\sim +20$ and -20 g cm^{-2} yr^{-1}, and this range is fairly independent of model ice sheet details (for instance, the full ice sheet retreat from 20 to 0 Kyears BP is achieved artificially in Fig. 10 by reducing the ice sheet volume inertia, but the mean ice sheet budget in this period is still ~ -20 g cm^{-2} yr^{-1}). What can change in the ice sheet environment to produce mean budgets of around -50 g cm^{-2} yr^{-1} between 14 and 9 Kyears BP, and also produce generally positive budgets *for the same ice sheet sizes* at times during the previous ~80 Kyears? (cf. Andrews, 1973).

It may be that the seasonal climate part of our model is too simplified. Additional non-linearities due to land–ocean longitudinal asymmetries, realistic atmospheric/oceanic dynamics and structure, day–night cycles, cloudiness and precipitation variations, etc., could possibly alter the model response to the orbital changes to occasionally give net northern ice sheet budgets of -50 g cm^{-2} yr^{-1} (e.g., between 14 and 9 Kyears BP), without increasing the amplitude of the intervening secondary oscillations of this paper. This possibility could perhaps best be tested by a higher powered GCM, although Hartmann and Short (1979) and North and Coakley (1979) have shown how longitudinal asymmetry can be included efficiently in simple climate models. Also Cess and Wronka (1979) suggest several new short-term feedbacks that could make simple climate model response more non-linear.

Alternatively, our seasonal climate model may be basically correct, and there may be other long-term processes in the system (apart from ice sheet volume inertia) with time scales of several Kyears or longer, as proposed by Eriksson (1968), Rooth et al. (1978) and others. These processes could result in the ice sheet budget depending not only on the current ice sheet size but also on its past sizes in the previous several Kyears, and so could distinguish between the positive and negative (-50 g cm^{-2} yr^{-1}) budgets at the same ice sheet size, as discussed above. Specific long-term pro-

cesses with this property include time-dependent lithospheric depression and/or non-plastic ice sheet flow (Emiliani and Geiss, 1957; Tanner, 1965), sudden jumps in the profiles of northern hemispheric and/or Antarctic ice sheets due to basal melting or sea incursions (Hollin, 1962; Wilson, 1964; Hughes, 1977; Thomas and Bentley, 1978), and deep ocean temperatures (Newell, 1974; Lemke, 1977; Saltzman, 1977). The inclusion of two or more long-term processes can produce free internal oscillations (e.g., Sergin, 1979), and it may be that such an oscillation is important for the full glacial–interglacial cycles.

Two other mechanisms related to the rapid ice sheet retreats are a possible layer of ice sheet meltwater covering a substantial part of the oceans (Adam, 1975; Berger et al., 1977; Emiliani et al., 1978), and extensive pro-glacial lakes causing calving at the feet of retreating ice sheets (Andrews, 1973). Processes such as these are not really long-term but through them the amount of ablation in one year can influence the ice sheet budgets in several succeeding years. This could cause a climatic flip-flop whereby once large ice sheets start to retreat, the oceanic meltwater layer and/or proglacial lakes increase and accelerate the retreat in succeeding years.

Before closing, we briefly discuss the relationship between Saltzman's (1977) approach and the present model. Saltzman shows that the dominant balance in the long-term global energy equation must be between three terms: global net radiation to or from space N, latent heat of fusion associated with the changing ice sheet mass F, and thermal energy of the global (~deep) oceans W. Newell (1974) has described a specific ice age mechanism involving these three quantities, and Mason (1976) has emphasized the similarity in order of magnitude between ice age variations of F and the variation of N (at mid and high latitudes) caused directly by the orbital perturbations. In our model we neglect W and our standard method of solution also neglects F, so that $N = 0$ and global and annual mean energy is exactly conserved in eq. (1). Therefore, all long-term energy residuals (which are generally much smaller than the seasonal energy terms) are neglected in eq. (1), and the long-term changes are parameterized by other exploratory equations. This method decreases the computer run-time considerably and has allowed a more extensive exploration of diagnostic snow and ice sheet parameterizations. However, during periods of rapid ice sheet retreat the average rate of release of ice sheet latent heat of fusion may be ~1/3 that of the insolation anomaly at mid and high latitudes due to the orbital perturbations (Mason, 1976), and so F should perhaps be included in eq. (1). We did include F in (1) for one run over the last 100 Kyears and found it caused very little difference in the response [a nearly constant 2° lat. equatorward shift from the solid curve in Fig. 3(b)]. This suggests that the "direct" effects of the orbital perturbations on the ice sheet budget (via the seasonal climate) are much larger than any "adjustments" required to satisfy the long-term energy equation, at least for the secondary oscillations.

Relatively simple models such as the present one are suitable for experimenting with ice age runs incorporating the various mechanisms mentioned above. The long-term energy residuals (N, F, and W above) can be explicitly incorporated in the model, but are not necessarily important for some mechanisms. If any mechanism is found that gives realistic glacial–interglacial cycles, the individual components and interactions could then be tested economically by higher powered GCMs (e.g., Gates, 1976a,b) and ice sheet models (e.g., Jenssen, 1977).

REFERENCES

Adam, D. P. 1975. Ice ages and the thermal equilibrium of the Earth, II. *Quat. Res. 5*, 161–171.

Andrews, J. T. 1973. The Wisconsin Laurentide ice sheet: dispersal centers, problems of rates of retreat, and climatic implications. *Arctic and Alpine Res. 5*, 185–199.

Andrews, J. T. 1975. *Glacial systems*. North Scituate, Mass.: Duxbury Press, 191 pp.

Barry, R. G., Andrews, J. T. and Mahaffy, M. A. 1975. Continental ice sheets: conditions for growth. *Science 190*, 979–981.

Beckinsale, R. P. 1973. Climatic change: a critique of modern theories. In *Climate in review* (ed. G. McBoyle). Boston: Houghton Mifflin, 132–151.

Berger, A. L. 1976. Obliquity and precession for the last 5,000,000 years. *Astron. and Astrophys. 51*, 127–135.

d high latitudes) caused directly by the rbations. In our model we neglect W, dard method of solution also neglects $V = 0$ and global and annual mean ctly conserved in eq. (1). Therefore, all ergy residuals (which are generally r than the seasonal energy terms) are eq. (1), and the long-term changes are d by other exploratory equations. This eases the computer run-time consider- allowed a more extensive exploration ic snow and ice sheet parameteri- ever, during periods of rapid ice sheet verage rate of release of ice sheet latent n may be ~1/3 that of the insolation mid and high latitudes due to the orbital s (Mason, 1976), and so F should ncluded in eq. (1). We did include F in un over the last 100 Kyears and found ry little difference in the response [a ant 2° lat. equatorward shift from the in Fig. 3(b)]. This suggests that the cts of the orbital perturbations on the get (via the seasonal climate) are much ny "adjustments" required to satisfy m energy equation, at least for the cillations.

simple models such as the present one for experimenting with ice age runs the various mechanisms mentioned ong-term energy residuals (N, F, and an be explicitly incorporated in the re not necessarily important for some If any mechanism is found that gives ial–interglacial cycles, the individual and interactions could then be tested by higher powered GCMs (e.g., .b) and ice sheet models (e.g., Jenssen,

ndrews, J. T. and Mahaffy, M. A. 1975. ice sheets: conditions for growth. *Science* 1.

P. 1973. Climatic change: a critique of ories. In *Climate in review* (ed. G. ston: Houghton Mifflin, 132–151.

976. Obliquity and precession for the last rs. *Astron. and Astrophys. 51*, 127–135.

Berger, A. L. 1978. Long-term variations of caloric insolation resulting from the Earth's orbital elements. *Quat. Res. 9*, 139–167.

Berger, W. H., Johnson, R. F. and Killingley, J. S. 1977. 'Unmixing' of the deep-sea record and the deglacial meltwater spike. *Nature 269*, 661–663.

Birchfield, G. E. 1977. A study of the stability of a model continental ice sheet subject to periodic variations in heat input. *J. Geophys. Res. 82*, 4909–4913.

Birchfield, G. E. and Weertman, J. 1978. A note on the spectral response of a model continental ice sheet. *J. Geophys. Res. 83*, 4123–4125.

Broecker, W. S. and Van Donk, J. 1970. Insolation changes, ice volumes and the O^{18} record in deep-sea cores. *Rev. Geophys. and Space Phys. 8*, 169–198.

Budyko, M. I. and Vasishcheva, M. A. 1971. Effect of astronomical factors on Quaternary glaciations (in Russian). *Meteorologija i Gidrologija 6*. 37–47.

Calder, N. 1974. Arithmetic of ice ages. *Nature 252*, 216–218.

Cess, R. D. and Wronka, J. C. 1979. Ice ages and the Milankovitch theory: a study of interactive climate feedback mechanisms. *Tellus 31*, 185–192.

Chorlton, J. C. and Lister, H. 1968. Snow accumulation over Antarctica. *I.A.S.H. 86*, 254–263.

CLIMAP Project Members. 1976, The surface of the ice-age Earth. *Science 191*, 1131–1137.

Coakley, Jr., J. A. 1979. A study of climate sensitivity using a simple energy balance model. *J. Atmos. Sci. 36*, 260–269.

Cogley, J. G. 1979. Albedo constrast and glaciation due to continental drift. *Nature 279*, 712–713.

Dickson, R. R. and Posey, J. 1967. Maps of snow-cover probability for the northern hemisphere. *Mon. Weath. Rev. 95*, 347–353.

Emiliani, C. 1978. The cause of the ice ages. *Earth and Planet. Sci. Lett. 37*, 349–354.

Emiliani, C. and Geiss, J. 1957. On glaciations and their causes. *Geologische Rundschau 46*, 576–601.

Emiliani, C., Rooth, C. and Stipp, J. J. 1978. The late Wisconsin flood into the Gulf of Mexico. *Earth and Planet. Sci. Lett. 41*, 159–162.

Emiliani, C. and Shackleton, N. J. 1974. The Brunhes epoch: isotopic paleo-temperatures and geochronology. *Science '83*, 511–514.

Eriksson, E. 1968. Air–ocean–icecap interactions in relation to climatic fluctuations and glaciation cycles. *Met. Monog. 8*, 68–92.

Evans, D. L. and Freeland, H. J. 1977. Variations in the Earth's orbit: pacemaker of the ice ages? *Science 198*, 528–530.

Flint, R. F. 1971. *Glacial and Quaternary geology*. New York: J. Wiley, 892 pp.

Gates, W. L. 1976a. Modeling the ice-age climate. *Science 191*, 1138–1144.

Gates, W. L. 1976b. The numerical simulation of ice-age-climate with a global general circulation model. *J. Atmos. Sci. 33*, 1844–1873.

Hantel, M. 1972. Polar boundary conditions in zonally averaged global climate models. *J. Appl. Meteor. 13*, 752–759.

Hartjenstein, G. and Efger, J. 1979. Linear parameterization of large-scale eddy transports. *Tellus 31*, 89–101.

Hartmann, D. L. and Short, D. A. 1979. On the role of zonal asymmetries in climate change. *J. Atmos. Sci. 36*, 519–528.

Hasselmann, K. 1976. Stochastic climate models. Part 1. Theory. *Tellus 28*, 473–485.

Hays, J. D., Imbrie, J. and Shackleton, N. J. 1976. Variations in the Earth's orbit: pacemaker of the ice ages. *Science 194*, 1121–1132.

Henderson-Sellers, A. and Meadows, A. J. 1979. The zonal and global albedos of the Earth. *Tellus 31*, 170–173.

Hollin, J. T. 1962. On the glacial history of Antarctica. *J. Glaciol. 4*, 173–195.

Hughes, T. 1977. West Antarctic ice streams. *Rev. Geoph. and Space Phys. 15*, 1–46.

Hunkins, K., Be, A. W. H., Opdyke, N. D. and Mathieu, G. 1971. The late Cenozoic history of the Arctic Ocean. In *Late Cenozoic glacial ages* (ed. K. K. Turekian). New Haven, Conn.: Yale Univ. Press, 215–238.

Imbrie, J. and Imbrie, K. P. 1979. *Ice ages: solving the mystery*. Short Hills, New Jersey: Enslow Publ., 224 pp.

Imbrie, J. and Imbrie, J. Z. 1980. Modelling the climatic response to orbital variations. *Science, 207*, 943–953.

Jenssen, D. 1977. A three-dimensional polar ice-sheet model. *J. Glaciol. 18*, 373–389.

Kominz, M. A. and Pisias, N. G. 1979. Pleistocene climate: deterministic or stochastic? *Science 204*, 171–172.

Ku, T. and Broecker, W. S. 1967. Rates of sedimentation in the Arctic Ocean, *Prog. Oceanogr. 4*, 95–104.

Kukla, G. J. 1975. Missing link between Milankovitch and climate. *Nature 253*, 600–603.

Lemke, P. 1977. Stochastic climate models, part 3. Application to zonally averaged energy models. *Tellus 29*, 385–392.

Lian, M. S. and Cess, R. D. 1977. Energy balance climate models: a reappraisal of ice-albedo feedback. *J. Atmos. Sci. 34*, 1058–1062.

Loewe, F. 1971. Considerations on the origin of the Quaternary icesheet of North America. *Arctic and Alpine Res. 3*, 331–344.

Lorenz, E. N. 1970. Climatic change as a mathematical problem. *J. Appl. Meteor. 9*, 325–329.

Lorenz, E. N. 1979. Forced and free variations of weather and climate. *J. Atmos. Sci. 36*, 1367–1376.

Mason, B. J. 1976. Towards the understanding and prediction of climatic variations. *Quart. J. Roy. Met. Soc. 102*, 473–498.

Meier, M. F. 1960. Distribution and variations of glaciers in the United States exclusive of Alaska. *I.A.S.H. 54*, 420–429.

Milankovitch, M. 1941. *Canon of insolation and the ice age problem.* Belgrade: Royal Serbian Academy, Special Publication *133*, 482 pp. Translated by Israel Program for Scientific Translation, Jerusalem, 1969.

Mock, S. J. 1967. Calculated patterns of accumulation on the Greenland ice sheet. *J. Glaciol. 6*, 795–803.

Newell, R. E. 1974. Changes in the poleward energy flux by the atmosphere and ocean as a possible cause for ice-ages. *Quat. Res. 4*, 117–127.

North, G. R. 1975. Theory of energy-balance climate models. *J. Atmos. Sci. 32*, 2033–2043.

North, G. R. and Coakley, Jr., J. A. 1979. Differences between seasonal and mean annual energy balance model calculations of climate and climate sensitivity. *J. Atmos. Sci. 36*, 1189–1204.

Paschinger, V. 1912. Die schneegrenze in verschiedenen klimaten. *Peterm. Georg. Mitt Erganz. 37*, 93 pp.

Paterson, W. S. B. 1969. *The physics of glaciers.* Oxford: Pergamon Press, 250 pp.

Paterson, W. S. B. 1972. Laurentide icesheet: estimated volumes during late Wisconsin. *Rev. Geophys. and Space Phys. 10*, 885–917.

Pollard, D. 1978. An investigation of the astronomical theory of the ice ages using a simple climate–icesheet model. *Nature 272*, 233–235.

Pollard, D. 1980. A simple parameterization for ice sheet ablation rate. *Tellus 32*, 384–388.

Rooth, C. G. H., Emiliani, C. and Poor, H. W. 1978. Climate response to astronomical forcing. *Earth and Planet. Sci. Lett. 41*, 387–394.

Ruddiman, W. F. and McIntyre, A. 1979. Warmth of the subpolar north Atlantic Ocean during northern hemispheric ice-sheet growth. *Science 204*, 173–175.

Saltzman, B. 1977. Global mass and energy requirements for glacial oscillations and their implications for mean ocean temperature oscillations. *Tellus 29*, 205–212.

Saltzman, B. and Vernekar, A. D. 1971. Note on the effect of Earth orbital radiation variations on climate. *J. Geophys. Res. 76*, 4195–4197.

Saltzman, B. and Vernekar, A. D. 1975. A solution for the northern hemispheric climatic zonation during a glacial maximum. *Quat. Res. 5*, 307–320.

Schneider, S. H. and Thompson, S. L. 1977. A surface temperature parameterization for zonal precipitation. *EOS 58*, 1144.

Schneider, S. H. and Thompson, S. L. 1979. Ice ages and orbital variations: some simple theory and modeling. *Quat. Res. 12*, 188–203.

Schuster, R. L. 1954. Project Mint Julep, part III. *U.S. Army Snow Ice and Permafrost Res. Est. Rep. 19*, 10 pp.

Schutz, C. and Gates, W. L. 1971 to 1974. *Global climatic data* R-915 (1971), R-915/1 (1972), R-1029 (1972), R-915/2 (1973), R-1317 (1973), R-1029/1 (1974), R-1425 (1974). A.R.P.A., Rand Corp., Santa Monica, Calif.

Sergin, V. Ya. 1979. Numerical modeling of the glaciers–ocean–atmosphere global system. *J. Geophys. Res. 84*, 3191–3204.

Shackleton, N. J., 1969. The last interglacial in the marine and terrestrial records. *Proc. Roy. Soc. London Ser. B. 174*, 135–154.

Shaw, D. M. and Donn, W. L. 1968. Milankovitch radiation variations: a quantitative evaluation. *Science 162*, 1270–1272.

Suarez, M. 1976. An evaluation of the astronomical theory of the ice ages. Ph.D. Thesis, Princeton Univ., 108 pp.

Suarez, M. J. and Held, I. M. 1976. Modelling climatic response to orbital parameter variations. *Nature, 263*, 46–47.

Suarez, M. J. and Held, I. M. 1979. The sensitivity of an energy balance climate model to variations in the orbital parameters. *J. Geophys. Res. 84*, 4825–4836.

Sugden, D. E. and John, B. S. 1976. *Glaciers and Landscape.* New York: J. Wiley, 376 pp.

Tanner, W. F. 1965. Cause and development of an ice age. *J. Geol. 73*, 413–430.

Thomas, R. H. and Bentley, C. R. 1978. A model for Holocene retreat of the West Antarctic ice sheet. *Quat. Res. 10*, 150–170.

Thompson, S. L. and Schneider, S. H. 1979. A seasonal zonal energy balance climate model with an interactive lower layer. *J. Geophys. Res. 84*, 2401–2414.

Van Loon, H. 1979. The association between latitudinal temperature gradient and eddy transport. Part 1: Transport of sensible heat in winter. *Mon. Weath. Rev. 107*, 525–534.

van Woerkom, A. J. J. 1953. The astronomical theory of climate changes. In *Climatic change—evidence, causes and effects* (ed. H. Shapley). Cambridge, Mass.: Harvard Univ. Press, 147–157.

Vernekar, A. D. 1972. Long-period global variations of incoming solar radiation. *Met. Monog. 12*, 1–20.

Warren, S. G. and Schneider, S. H. 1979. Seasonal simulation as a test for uncertainties in the parameterizations of a Budyko–Sellers climate model. *J. Atmos. Sci. 36*, 1377–1391.

Weertman, J. 1961. Stability of ice-age icesheets. *J. Geophys. Res. 66*, 3783–3792.

Weertman, J. 1964. Rate of growth or shrinkage of nonequilibrium icesheets. *J. Glaciol. 5*, 145–158.

Weertman, J. 1976. Milankovitch solar radiation variations and ice age ice sheet sizes. *Nature 261*, 17–20.

White, G. H. 1976. Climatic feedbacks calculated from satellite observations. G.F.D. Summer Study Program, Woods Hole Oceanog. Inst., 168–190.

Williams, J. H. 1974. Simulation of the atmospheric circulation using the NCAR global circulation model with present day and glacial period boundary conditions. Ph.D. Thesis, Univ. of Colorado, Boulder, 328 pp.

V. Ya. 1979. Numerical modeling of the
-s–ocean–atmosphere global system. *J. Geo-*
Res. 84, 3191–3204.
on, N. J., 1969. The last interglacial in the
and terrestrial records. *Proc. Roy. Soc.*
n Ser. B. 174, 135–154.
M. and Donn, W. L. 1968. Milankovitch
on variations: a quantitative evaluation. *Science*
270–1272.
M. 1976. An evaluation of the astronomical
of the ice ages. Ph.D. Thesis, Princeton Univ.,
M. J. and Held, I. M. 1976. Modelling climatic
se to orbital parameter variations. *Nature, 263*,

M. J. and Held, I. M. 1979. The sensitivity of an
balance climate model to variations in the
parameters. *J. Geophys. Res. 84*, 4825–4836.
D. E. and John, B. S. 1976. *Glaciers and*
cape. New York: J. Wiley, 376 pp.
V. F. 1965. Cause and development of an ice
Geol. 73, 413–430.
R. H. and Bentley, C. R. 1978. A model for
ne retreat of the West Antarctic ice sheet.
Res. 10, 150–170.
n, S. L. and Schneider, S. H. 1979. A seas-
nal energy balance climate model with an
ive lower layer. *J. Geophys. Res. 84*, 2401–

. H. 1979. The association between latitudinal
ture gradient and eddy transport. Part 1:
ort of sensible heat in winter. *Mon. Weath.*
7, 525–534.
rkom, A. J. J. 1953. The astronomical theory of
changes. In *Climatic change—evidence,*
and effects (ed. H. Shapley). Cambridge,
Harvard Univ. Press, 147–157.
A. D. 1972. Long-period global variations of
g solar radiation. *Met. Monog. 12*, 1–20.
S. G. and Schneider, S. H. 1979. Seasonal
ion as a test for uncertainties in the para-
ations of a Budyko–Sellers climate model. *J.*
Sci. 36, 1377–1391.
. J. 1961. Stability of ice-age icesheets. *J.*
s. Res. 66, 3783–3792.
. J. 1964. Rate of growth or shrinkage of
librium icesheets. *J. Glaciol. 5*, 145–158.
, J. 1976. Milankovitch solar radiation varia-
l ice age ice sheet sizes. *Nature 261*, 17–20.
H. 1976. Climatic feedbacks calculated from
observations. G.F.D. Summer Study Pro-
oods Hole Oceanog. Inst., 168–190.
J. H. 1974. Simulation of the atmospheric
on using the NCAR global circulation model
esent day and glacial period boundary con-
Ph.D. Thesis, Univ. of Colorado, Boulder, 328

Williams, L. D. 1978. Ice-sheet initiation and climatic influences of expanded snow cover in Arctic Canada. *Quart. Res. 10*, 141–149.

Wilson, A. T. 1964. Origin of ice ages: an ice shelf theory for Pleistocene glaciation. *Nature 201*, 147–149.

Yapp, C. J. and Epstein, S. 1977. Climatic implications of D/H ratios of meteoric water over North America (9500–22,000 B.P.) as inferred from ancient wood cellulose C–H hydrogen. *Earth and Planet. Sci. Lett. 34*, 333–350.

РЕАКЦИЯ ЗОНАЛЬНОЙ КЛИМАТИЧЕСКОЙ МОДЕЛИ С ЛЕДНИКОВЫМИ ЩИТАМИ НА ОРБИТАЛЬНЫЕ ВОЗМУЩЕНИЯ В ТЕЧЕНИЕ ЧЕТВЕРТИЧНЫХ ЛЕДНИКОВЫХ ПЕРИОДОВ

При помощи простой климатической модели, явно описывающей ледниковые щиты, исследуется астрономическая теория ледниковых периодов. Одноуровенная зонально осредненная сезонная энергобалансовая модель решается численно с определением температуры на уровне моря как функции широты и месяца (подобно Норсу, 1975). Снеговой покров, меняющийся с сезоном (что влияет на планетарное альбедо) включен диагностически путем простых параметризаций ежемесячных выпадений и таяний снега. Полные годовые накопления и абляция на поверхности ледниковых щитов на каждой широте вычисляются с теми же параметризациями, что и для снега (с температурой, учитывающей высоту щита при вертикальном градиенте $-6{,}5°C\ км^{-1}$). Рассмотрение ледниковых щитов следует Уиртману (1976), где течение льда аппроксимируется как течение идеально пластичной жидкости, что ограничивает профиль щита параболой. Ледяной щит северного полушария простирается к экватору от 75°с.ш. (что соответствует береговой линии Северного ледовитого океана).

Модельные кривые для последних 100 тыс.лет рассчитаны вычислениями годичной «погоды», как описано выше, для каждых 2 тыс.лет с инсоляцией, взятой с учетом реальных возмущений параметров земной орбиты. Изменения в размерах ледникового щита для каждого шага в 2 тыс.лет зависят только от ежегодного баланса снега, проинтегрированного по всей поверхности щита. В этих расчетах южная граница ледяного щита северного полушария колеблется в пределах 7° широты, что правильно моделирует фазы и приблизительные амплитуды высокоустотных компонент (43 и 22 тыс.лет) данных глубоководных осадков (Хэйс и др., 1976). Однако модель неспособна воспроизвести основные ледниковые циклы (от 100 до 120 тыс.лет) этих данных. Описана чувствительность модельных расчетов к изменениям различных ее параметров, но ни одно из этих изменений не улучшает существенно сходимости расчетных кривых к упомянутым данным. В заключение мы обсуждаем типы механизмов, которые могли бы дать реалистические ледниковые циклы.

Tellus (1980) *32*, 384–388

SHORT CONTRIBUTION

A simple parameterization for ice sheet ablation rate[1]

By DAVID POLLARD, *Division of Geological and Planetary Sciences, California Institute of Technology, Pasadena, California 91125, U.S.A.*

(Manuscript received January 8, 1980)

ABSTRACT

A parameterization of monthly mean ice sheet ablation as a function only of surface air temperature and insolation is examined. By considering differences in summer climate between the present and the last ice age, it is suggested that the parameterization adequately describes long-term changes in ablation. Although significant discrepancies are found between the parameterization and the seasonal variation of ablation observed on present-day glaciers, the seasonal ablation cycle is still predicted accurately enough to maintain the validity of the parameterization for long-term net annual variations.

1. Introduction

Several recent models of northern hemispheric ice sheet fluctuations during the last $\sim 10^6$ years have used relatively simple parameterizations of ablation on the ice sheet surfaces (Weertman, 1976; Sergin, 1979; Pollard et al., 1980). The process of ablation is an important part of the climatic control over the size of present-day glaciers, and ablation variations in the past could have been important in controlling the past ice sheet fluctuations. Ablation is used here to mean "the reduction in mass of a vertical ice sheet column due to the removal of H_2O out of the column by surface processes"; calving into oceans is excluded. In practice ablation mostly involves melting and subsequent runoff in surface or basal streams during summer, but can also involve evaporation or wind-drifting. The full process is complex and is described in Paterson (1969, Ch. 4) and Sugden and John (1976, Ch. 14).

In Pollard et al. (1980) the monthly mean ablation, A, at any point on the ice sheet surface is parameterized in the form

$$A = \max[0; aT + bQ + c] \qquad (1)$$

where T is the monthly mean surface air temperature (corrected for ice sheet elevation above sea-level using a constant atmospheric lapse rate), Q is the monthly mean insolation at the top of the atmosphere, and a, b, and c are constants. For non-zero A, (1) is basically a linearized energy-balance equation for a melting surface with no heat capacity; somewhat more complex parameterizations involving more climatic variables were first developed in the glaciological literature (e.g., Sverdrup, 1935). Of course more sophisticated snowmelt models are in current use, and a few have recently been applied to paleoglaciological problems (e.g. Williams, 1979).

This note examines the adequacy of such a simple parameterization as (1) for ice age models. In Section 2 past ablation variations for a given month (July) are considered, and found to be adequately describable in terms of T alone. However ablation typically has a large non-linear seasonal variation and is negligible in winter, making it important to "choose" the right months of the year to compare with past eras, i.e., to correctly predict the beginning and end of the main ablation season. In Section 3 some discrepancies are found between present-day seasonal observations and a parameterization of the same type as (1), but the scatter is only equivalent to a relatively small error ($\sim \pm 1$ month) in the phase of the seasonal ablation cycle. The purpose of including Q in (1) and the numerical values for a, b and c are discussed in Section 4.

[1] Contribution number 3374 of the Division of Geological and Planetary Sciences, California Institute of Technology, Pasadena, California 91125, U.S.A.

0040-2826/80/040384-05$02.50/0 © 1980 Munksgaard, Copenhagen

2. Variations in past eras

Ablation depends not only on surface air temperature and insolation but also on cloud cover, wind speed, relative humidity and on physical properties of the surface itself. Each of these parameters has probably varied systematically over synoptic scales in past eras and so could potentially be important for ice age ablation parameterizations. One approach of estimating the relative importance of the meteorological parameters (cf Coakley, 1977) is shown in Table 1. The Δp values in column 2 represent differences in the parameter p between the present July and July 18 Kyear BP on continents around ~50° N, estimated from the GCM results of Gates (1976). These summer values are the most relevant to the net annual ablation, since by far the most ablation occurs in the summer months. The values of the partial derivatives $\partial A/\partial p$ in column 3 are estimated from the theoretical "free ablation" graphs of Kraus (1975), and represent the regions of these graphs in which the bulk of ablation occurs on real glaciers (i.e., by melting with air temperature $\gtrsim 0$ °C); these values are consistent with earlier semi-empirical ablation formulae (e.g., Sverdrup, 1935). They are calculated for a standard glacier surface (with albedo 0.5) in "steady-state" ablation, i.e., with no sensible heat storages and with all ablated water removed immediately. [The partial derivatives for T and Q correspond to a and b in (1), and their values are considered further in Sections 3 and 4.]

The magnitudes of the products in column 4 indicate that by far the largest ablation rate changes of past eras have been caused by the changes in surface air temperature, T. This suggests that a parameterization in terms of T alone would be adequate for an ice age model; (actually the next most important variable, surface wind speed, could not realistically be predicted in simple one-layer climate models).

It should be noted that the Δp values in Table 1 are averages over many days, but the steady-state partial derivatives take no account of the pronounced non-linear daily cycles involved in real ablation situations. However in situations where melting is occurring for a significant fraction f of each day, one would expect that the inclusion of these day–night effects would reduce the products in column 4 by factors of between $\sim f$ and ~ 1, and would not seriously affect their relative magnitudes.

Table 1 also neglects any systematic changes in properties of the ice sheets themselves. For instance sub-zero internal temperatures can cause meltwater to refreeze elsewhere in the ice sheet and not run off; the winter cold-wave of seasonal heat in near-surface layers can significantly inhibit ablation (Muller, 1963). There is little or no direct evidence of such systematic changes as ice sheet size varied in the past, but these properties do vary widely on

Table 1. *Effect of past variations Δp of summer climate on ablation rate A*

Parameter p	Δp (ice age July minus present July)	$\partial A/\partial p$ in (g cm^{-2} month^{-1} per units of col. 1)	Δp ($\partial A/\delta p$) in (g cm^{-2} month^{-1})
Surface air temperature, T (°C)	−10	15	−150
Insolation, Q (W m^{-2})	±15*	(0.8) × (0.4) = 0.32†	±5
Total cloudiness (areal fraction)	+0.2	Effect of sunlight absorbed: (0.8) × (−70) = −56†	−11
		Effect of net IR: (−0.8) × (−80) = 64‡	+13
Surface wind speed (m s^{-1})	+2	15	+30
Relative humidity (%)	+10 (at 800 mb level)	1	+10

* Representative not of July 18 Kyears BP but of the general magnitude of past variations in mean summer insolation at ~50° N due to the orbital perturbations (e.g., Vernekar, 1972).

† Factor of (0.8) represents ablation per sunlight absorbed by the glacier surface (Kraus, 1975); factors of (0.4) and (−70) represent changes in sunlight absorbed per change in the relevant parameter p as computed by Schneider and Dickinson (1976, table 1) allowing for multiple reflections between cloud deck and surface.

‡ Factor of (−0.8) represents ablation per net infrared radiation lost by the glacier surface to the atmosphere (Kraus, 1975); factor of (−80) represents an average sensitivity of this infrared loss to various types of cloud cover as determined by glacial field measurements (Wallen, 1948; Lister and Taylor, 1961).

present glaciers and ice caps (Paterson, 1969, Ch. 2). Such properties can be predicted only by relatively complex ice sheet models, and are effectively assumed constant in most simple ice age simulations.

3. Present-day observations

In this century considerable glaciological fieldwork has been devoted to relating the ablation on glaciers and ice caps to the local meteorological conditions (e.g., Paterson, 1969, Ch. 4). Schytt (1967) and Loewe (1971) among others have compiled sets of present-day glacial data and plotted ablation rate, A, against surface air temperature, T, averaged through most or all of the ablation season, i.e., ~May to ~September. (Insignificant ablation occurs in winter months outside of the ablation season.) For interannual variations on individual glaciers, the relationship is good and shows $\partial A/\partial T$ ~10 (g cm^{-2} month^{-1}) per (°C); however there is considerable scatter between glaciers in different types of climates (e.g., continental versus maritime), and also between measurements averaged only over a few weeks or less on the same glacier. Much of this scatter in the relationship between A and T is probably due to seasonal and latitudinal variations of insolation and also due to variations in surface albedo, which can change seasonally from ~0.8 (fresh snow) to ~0.5 (melting ice) (e.g., Wallén, 1948). These variations would correspond to ablation rate variations of ~100 g cm^{-2} month^{-1} in column 4 of Table 1.

In Fig. 1 we have attempted to improve the ablation parameterization by adding a second variable "net radiation absorbed", R, which primarily contains the effects of insolation, surface albedo and also cloudiness. As far as an accurate representation of this data is concerned, the result shown is basically negative; the considerable scatter in the relationship between A and T has been reduced only slightly if at all by the addition of the second variable R. The scatter in the figure must be due to some combination of observational error, seasonal and interglacial variability of ice body properties such as seasonal heat storage and refreezing, and also due to the exaggerated point-to-point variability of surface wind speed and relative humidity for measurements averaged only over a few days. Unfortunately even if these effects were resolvable from the available data, a realistic treatment of these variables (and also of seasonally varying surface albedo contained in the variable R) is beyond the scope of most simple ice age models.

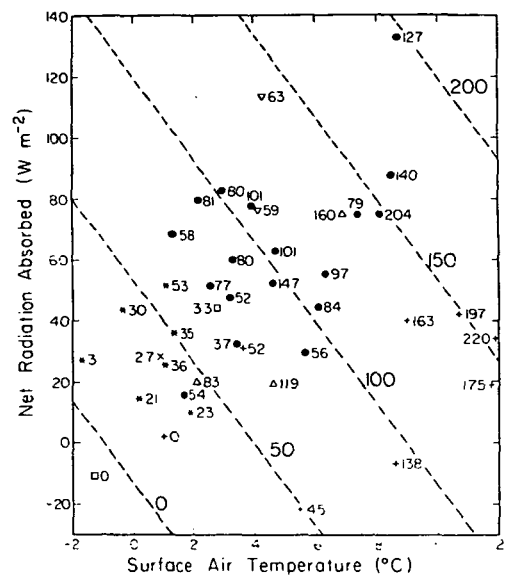

Fig. 1. Measurements of present-day ablation vs surface air temperature, T, and net solar and infrared radiation absorbed, R. Values adjacent to each point are ablation rates, A, in g cm^{-2} month^{-1}. The measurements are averaged over a whole number of days during the ablation season. The figure contains all the data we found where simultaneous determinations of daily mean A, T, and R were published. The general level of observational error for each variable (not often reported) may be $\lesssim$10% of the total range in the figure. The sources for the various points in the figure are: • Kårsa Glacier (Wallén, 1948); + Hoffells. Glacier (Ahlmann and Thorarinsson, 1938); * Isaschen. Ice Cap (Sverdrup, 1935); △ Sveanor Snowfield (Sverdrup, 1935); ▽ Britannia Glacier (Lister and Taylor, 1961); × Barnes Ice Cap (Ward and Orvig, 1953): ⊡ Kessel. Snowfield (Ambach and Hoinkes, 1963). The dashed lines of constant ablation rate show a "fit" that corresponds to the parameterization in the text.

The level of scatter from the linear fit in Fig. 1 is $\lesssim\pm$50 g cm^{-2} month^{-1}. This is equivalent to ~$\pm$5 °C in air temperature, which is much less than the full seasonal variation at any one location and is comparable to the change through one month in spring or autumn. Therefore the beginning and end of the main ablation season could be

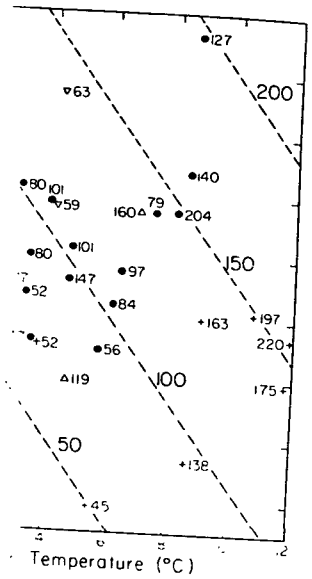

present-day ablation vs surface
et solar and infrared radiation
ent to each point are ablation
ith^{-1}. The measurements are
number of days during the
contains all the data we found
inations of daily mean A, T,
general level of observational
not often reported) may be
the figure. The sources for the
ure are: • Kårsa Glacier
lls. Glacier (Ahlmann and
aschen. Ice Cap (Sverdrup,
field (Sverdrup, 1935); ▽
nd Taylor, 1961); × Barnes
1953): ⊡ Kessel. Snowfield
963). The dashed lines of
a "fit" that corresponds to
xt.

ately even if these effects
available data, a realistic
les (and also of season-
edo contained in the
cope of most simple ice

the linear fit in Fig. 1 is
This is equivalent to
e, which is much less
ion at any one location
change through one
. Therefore the begin-
lation season could be

predicted to within ~1 month by a parameterization in terms of T alone, with a non-linear cutoff below $T \lesssim -5\,°C$ to represent negligible ablation in winter.

4. Parameterization

Although the radiative variable R has not eliminated the scatter in Fig. 1, it still seems preferable to include the seasonal variation of Q in an ablation parameterization for the following reason: with all other variables held constant, the full winter–summer variation of Q would certainly affect ablation as much as a variation in T of ~10°C, and so the inclusion of Q should slightly improve the predicted phase of the seasonal cycle.

Numerical values for (1) are chosen below, but one should note that these values are constrained only within wide limits by the data in this paper, and the main point is the basic form of (1). As in Table 1, we estimate $\partial A/\partial Q$ ~0.3 (g cm^{-2} month^{-1}) per (W m^{-2}). (This steady-state derivative should be affected only slightly by day–night effects since the daily cycle of insolation is roughly correlated with that of ablation.) Using the value of $\partial A/\partial T$ from present-day interannual variations (Section 3), this yields the following equation for monthly mean quantities:

$$A\ (\mathrm{g\ cm^{-2}\ month^{-1}}) \approx \max[0;\ 10T\,(°\mathrm{C}) + 0.3Q\,(\mathrm{W\ m^{-2}}) - 50] \qquad (2)$$

We have estimated the constant "50" in (2) by comparison with the data in Fig. 1, using R (W m^{-2}) = $0.4Q - 80$. [The factor 0.4 allows for multiple reflections off a ~0.3 cloud cover (Schneider and Dickinson, 1976), and 80 W m^{-2} represents net infrared loss from a melting surface with this cloud cover (Lister and Taylor, 1961).] The corresponding linear fit is shown in the figure. This constant "50" in (2) is also consistent with the general observation that significant ablation occurs only where the monthly mean temperature rises much above ~−7 °C in summer (e.g., Orvig, 1954; Bull and Carnein, 1968). The non-linear cutoff in (2), basically due to the transition from melting to evaporation, corresponds to the non-linear temperature dependence (roughly T^2 to T^3) suggested by Ahlmann (1948).

In summary, one should expect significant discrepancies between eq. (2) and present observed seasonal cycles of ablation. Much of this discrepancy could be due to seasonal variations of surface albedo, but Fig. 1 shows that other factors (e.g., seasonal heat storage) are significant. However, any such seasonal discrepancy should not be serious for the ice age problem as long as the summer months during which most ablation occurs are predicted reasonably well. This is because Table 1 shows that for these months the past variations of ablation rate have been controlled by past variations of surface air temperature, consistent with eq. (2).

REFERENCES

Ahlmann, H. W. 1948. Glaciological research on the North Atlantic coasts. *Roy. Geog. Soc., London. Res. Ser. 1*, 83pp.

Ahlmann, H. W. and Thorarinsson, S. 1938. Vatnajökull scientific results of the Swedish Icelandic investigations 1936–37–38. Ch. V. *Geogr. Annal. 20*, 171–233.

Ambach, W. and Hoinkes, M. 1963. The heat balance of an alpine snowfield. *I.A.S.H. 61*, 24–36.

Bull, C. and Carnein, C. R. 1968. The mass balance of a cold glacier: Meserve glacier, south Victoria Land, Antarctica. *I.A.S.H. 86*, 429–446.

Coakley, Jr., J. A. 1977. Feedbacks in vertical-column energy balance models. *J. Atmos. Sci. 34*, 465–470.

Gates, W. L. 1976. The numerical simulation of ice-age climate with a global general circulation model. *J. Atmos. Sci. 33*, 1844–1873.

Kraus, H. 1975. An energy balance model for ablation in mountainous areas. *I.A.S.H. 104*, 74–82.

Lister, H. and Taylor, P. F. 1961. Heat balance and ablation of an Arctic glacier. *Meddel. om Grönland 158*, 1–54.

Loewe, F. 1971. Considerations on the origin of the Quaternary icesheet of North America. *Arctic and Alpine Res. 3*, 331–344.

Muller, F. 1963. Englacial temperature measurements on Axel Heiberg Island, Canadian Arctic Archipelago. *I.A.S.H. 61*, 168–180.

Orvig, S. 1954. Glacial-meteorological observations on icecaps in Baffin Island. *Geogr. Annal. 36*, 193–318.

Paterson, W. S. B. 1969. *The physics of glaciers*. Oxford: Pergamon Press, 250 pp.

Pollard, D., Ingersoll, A. P. and Lockwood, J. G. 1980. Response of a zonal climate–ice sheet model to the orbital perturbations during the Quaternary ice ages. *Tellus 32*, 301–319.

Schneider, S. H. and Dickinson, R. E. 1976. Parameterization of fractional cloud amounts in climate

models: the importance of modeling multiple reflections. *J. Appl. Met. 15*, 1050–1056.

Schytt, V. 1967. A study of "ablation gradient". *Geogr. Annal. 49A*, 327–332.

Sergin, V. Ya. 1979. Numerical modeling of the glaciers–ocean–atmosphere global system. *J. Geophys. Res. 84*, 3191–3204.

Sugden, D. E. and John, B. S. 1976. *Glaciers and landscape*. New York: J. Wiley, 376 pp.

Sverdrup, H. U. 1935. Scientific results of the Norwegian–Swedish Spitsbergen expedition in 1934. Part IV. *Geogr. Annal. 17*, 145–166.

Vernekar, A. D. 1972. Long-period global variations of incoming solar radiation. *Met. Monog. 12*, 1–20.

Wallén, C. C. 1948. Glacial-meterological investigations on the Kårsa glacier in Swedish Lapland. *Geogr. Annal. 30*, 451–672.

Ward, W. H. and Orvig, S. 1953. The glaciological studies of the Baffin Island expedition, 1950. Part IV. *J. Glaciol. 2*, 158–168.

Weertman, J. 1976. Milankovitch solar radiation variations and ice age ice sheet sizes. *Nature 261*, 17–20.

Williams, L. D. 1979. An energy balance model of potential glacierization of northern Canada. *Arctic and Alpine Res. 11*, 443–456.

Reprinted from Preprint Volume: Fifth Conference on Atmospheric Radiation, October 31–4 November 1983, Baltimore, Maryland. Published by the American Meteorological Society, Boston, Mass.

10A.29R

EMPIRICAL RELATIONS BETWEEN RADIATIVE FLUX, CLOUDINESS, AND OTHER METEOROLOGICAL PARAMETERS

D.D. Wenkert and A.P. Ingersoll
California Institute of Technology
Pasadena, California

1. INTRODUCTION

We are analyzing Earth Radiation Budget (ERB) data obtained by the scanning, narrow field-of-view channels of the ERB instrument on Nimbus 7 from the whole Earth for six days in June 1979. Using meteorological information from the FGGE Level IIIb (ECMWF) data set and cloudiness information from the THIR instrument onboard Nimbus 7, we calculate statistical relations between the angularly resolved radiances measured by ERB and various meteorological and cloud parameters. These relations are then combined to determine relations between angularly integrated visible and infrared upwelling flux (irradiance) and meteorological parameters (including cloudiness).

We are using the relationships we obtain between radiative flux and other atmospheric variables in three ways. The effect of varying cloudiness on the net flux at the top of the atmosphere is being determined. Various different radiation parameterizations, appropriate for simple climate models, are being developed. Finally, relationships between radiation and other atmospheric variables are being defined, against which the internal statistics of general circulation models may be tested. In this paper, we report on some preliminary results oriented primarily toward solving the first problem.

2. OBSERVATIONS

The radiation data consist of angularly resolved, broad band measurements of infrared and visible radiation obtained by the four scanning telescopes of the ERB instrument on the Nimbus 7 satellite, which travels in a sun-synchronous noon-midnight orbit. At any given time, the scanners were capable of sampling most of the Earth's visible disc with instantaneous fields of view of 0.25 degrees x 5.12 degrees (Jacobowitz et al., 1978). The data are archived on Sub Target Radiance Tapes (STRT's, see Stowe and Fromm, 1983), where they are organized by target area (TA, a roughly square region on Earth about 500 km on a side; there are 2070 of them), sub target area (there are nine of these in each TA), time of day, and viewing geometry. Also included on the STRT are information on the type of surface found in each TA and STA, and cloudiness information for the STA's (when available) obtained by the THIR instrument on Nimbus 7 (Chen et al., 1980).

The meteorological information we use comes from the 6-hourly global synoptic analyses, produced as a Level IIIb data set by the European Center for Medium-range Weather Forecasting (ECMWF) for the second Special Observing Period of FGGE. This data set has space and time resolutions that match quite well those of the ERB data.

3. STATISTICAL ANALYSIS

In general, the upwelling flux, F, from a region is related to the upwelling radiance field, R, by

$$F(\mu_o) = \int_{2\pi}\int R(\theta,\phi;\mu_o)\cos\theta\, d\theta\, \sin\theta\, d\phi,$$

where μ_o = cosine of solar zenith angle, θ = zenith angle of observer, ϕ = relative azimuth from sun to observe. We have divided the upward hemisphere into 32 discrete angular bins for the visible radiances and 14 angular bins for the infrared. Thus the relation between flux and radiance becomes

$$F(\mu_o) = \sum_i R_i(\mu_o)\,\mu_i\,\Omega_i \quad ,$$

where μ_i = cosine of zenith angle in ith bin, Ω_i = size of ith angular bin in steradians. It is simple to show, given any variable x, that

$$\sigma_{xF} = \sum_i \sigma_{xRi}\,\mu_i\,\Omega_i$$

where σ_{xF} = covariance of x and F (flux), σ_{xRi} = covariance of x and R_i (radiance in ith bin). Similarly,

$$\sigma_F^2 = \sum_i\sum_j \sigma_{RiRj}\,\mu_i\,\Omega_i\,\mu_j\,\Omega_j \quad ,$$

where σ_F^2 = variance of flux σ_{RiRj} = covariance of radiance in ith bin and radiance in jth bin.

It is not necessary to measure the entire upwelling radiation field each time to determine statistical relationships between upwelling flux and other parameters. All that is necessary is that covariances of the parameter in question with the radiances of all the angular bins be obtained and that covariances of the radiance in each angular bin with the radiances in each of the other bins be known. If at least a few times during the period under investigation the radiance in each bin has been measured at the same time (i.e., within the same time averaging interval) as the radiance in any given other bin, and if the same is true for the radiance in each bin and each of the meteorological (and cloudiness) parameters in which we are interested, then we have sufficient information to deduce statistical relations between the upwelling radiative flux and the parameters of interest.

For the investigations discussed here we are interested in the diurnally averaged radiative flux rather than the flux at one specific solar zenith angle. Since the ERB instrument takes data only near local noon and local midnight, this can be a problem for visible radiance measurements. If we let $\overline{x}$ be the diurnal average of x, and let t be the time of day then

$$F(\mu_o(t)) = \sum_i R_i(\mu_o(t))\ \mu_i \Omega_i \quad ,$$

and

$$\overline{F} = \sum_i \overline{R_i}\ \mu_i\ \Omega_i .$$

We can define a bidirectional reflectance such that

$$R_i(t) = \mu_o(t)\ A_i(t)\ F_o/\pi \quad ,$$

where F_o = solar flux (solar constant), $A_i(t) = A_i(\mu_o(t),s)$ = bidirectional reflectance for a cloud and surface type s, for a cosine of solar zenith angle μ_o, in the ith outgoing angular bin. Now we can use

$$\overline{R_i} = \overline{\mu_o A_i}\ F_o/\pi = (\overline{\mu_o A_i}/\mu_o(t)\ A_i(t))\ R_i(t) \quad .$$

If we know the way in which the bidirectional reflectance varies with solar zenith angle then it is no problem to determine the diurnally averaged visible radiance from an observed instantaneous visible radiance. For the results reported here, we have assumed that in all cases A_i was independent of μ_o. Thus we used

$$\overline{R_i} = (\overline{\mu_o}/\mu_o(t))\ R_i(t) \quad .$$

Note that $\overline{\mu_o}$ is a known function of latitude and time of year and $\mu_o(t)$ is listed in the STRT records for all observations. The averaging interval we use for our data is 24 hours and the averaging region is a full Target Area (c. 500 km square). However, we do not average in any visible radiances measured for regions in darkness. It is hoped that the scheme outlined above provides good diurnal averages for visible radiances and that averaging both the near noon and near midnight values of infrared radiances provides good diurnal averages for those. Using standard linear multiple regression, the variances and covariances of radiative fluxes and other parameters yield empirical equations relating these variables to each other.

4. RESULTS

In Table 1, we have listed the coefficients for single parameter regressions of the different (diurnally averaged) radiative fluxes against 1000 mbar temperature and against fractional cloudiness (as determined by THIR). The net flux (Fnet) is simply the average incident solar flux minus the sum of the outgoing visible and infrared fluxes. The regressions were determined from the data set for one day (12 June 1979) for the various regions of the Earth listed. The single parameter regression coefficients are equivalent to total derivatives of the flux with respect to the appropriate parameter (either T1000 or Xcld). Thus the variation in radiation due to cloudiness or surface air temperature, listed in this table reflect the actual distributions of cloudiness or surface air temperature on 12 June 1979. To determine the effect, for example, of varying cloudiness while holding latitude and surface air temperature constant, a multiparameter regression should be performed. In order to get an idea of the magnitude of the different variations in radiation due to a change in cloudiness or temperature, we have listed, in Table 2, the change in flux due to a positive change in T1000 or Xcld of one standard deviation. These are compared to the standard deviations of the fluxes. It is clear from these tables, that on 12 June 1979 higher cloudiness was associated with effects on outgoing terrestrial radiation and reflected solar radiation that nearly cancel when averaged over the entire Earth. This near cancellation is also seen in the data sets for most of the other five days investigated, and it shows up in multiparameter regressions involving cloudiness. Therefore we believe this effect is real. The breakdown of the cloudiness effect by latitude band is enlightening. The effect of clouds on emission dominates in those regions receiving little insolation (i.e., the winter hemisphere) and the albedo effect dominates in regions receiving more sunlight (i.e. the summer hemisphere). The net result over the globe is near cancellation. Increased surface air temperature is associated with decreased net flux over most of the globe, presumably because of increased thermal emission with increasing temperature. Interestingly, however, this relationship breaks down in some regions, specifically the tropics. Perhaps in this region, increasing surface temperatures lead to increasing atmospheric humidity and penetrative convective cloudiness, both leading to a higher atmospheric opacity.

5. CONCLUDING REMARKS

The Nimbus 7 ERB data set can be used along with correlative data to investigate the effects of varying cloudiness and meteorology on the radation budget of the atmosphere, without using any a priori assumptions or angular models. However, to properly correct for the probable systematic underestimation of diurnally averaged upwelling visible flux, due to collection of visible ERB data at the lowest solar zenith angles (corresponding to noontime) for each target, some assumptions about angular models must be made. We are presently developing various diurnal corrections which involve a minimum of assumptions. We are also investigating

the effects of different averaging intervals (of area and time) and different divisions of the upward hemisphere into angular bins on our statistics. We hope to thereby make more robust our findings on the relationships between cloudiness, meteorology, and atmospheric radiation, including the apparently neutral effect of clouds on the Earth's radiation budget.

6. REFERENCES

Chen, T. S., L. L. Stowe, V. R. Taylor, and P. F. Clapp, 1980: Classification of clouds using THIR data from the Niumus-7 satellite, Proceedings International Radiation Symposium, Fort Collins, CO, p.315-317.

Jacobowitz, H., L. L. Stowe, and J. R. Hickey, 1978: The earth radiation budget (ERB) experiment, The Nimbus 7 User's Guide, NASA Goddard Space Flight Center, p.33-69.

Stowe, L. L., and M. D. Fromm, 1983: The Nimbus 7 ERB Sub Target Radiance Tape (STRT) data base, NOAA Technical Memorandum, in press.

Table 1.

Coefficients for single parameter regressions

Region	Parameter	Fvis	Fir	Fnet
90.0S-67.5S	T1000	0.000E+00	3.205E+00	-3.205E+00
	Xcld	0.000E+00	-5.881E-01	5.881E-01
67.5S-45.0S	T1000	2.394E+00	1.455E+00	-3.849E+00
	Xcld	1.552E+01	-6.315E+01	4.763E+01
45.0S-22.5S	T1000	5.914E-01	2.843E+00	-3.435E+00
	Xcld	4.608E+01	-8.768E+01	4.160E+01
22.5S-0.0	T1000	1.411E+00	-4.457E+00	3.045E+00
	Xcld	6.335E+01	-6.589E+01	2.541E+00
0.0-22.5N	T1000	-9.079E-01	-2.590E+00	3.498E+00
	Xcld	8.097E+01	-1.321E+02	5.111E+01
22.5N-45.0N	T1000	-2.781E+00	3.571E+00	-7.902E-01
	Xcld	7.182E+01	-1.024E+02	3.060E+01
45.0N-67.5N	T1000	-7.308E+00	2.204E+00	5.104E+00
	Xcld	1.870E+02	-7.299E+01	-1.140E+02
67.5N-90.0N	T1000	-4.846E+00	5.602E-01	4.286E+00
	Xcld	2.026E+02	-6.178E+01	-1.409E+02
Whole Earth	T1000	6.241E-01	2.552E+00	-3.176E+00
	Xcld	8.991E+01	-8.402E+01	-5.884E+00

Table 2.
Effects on radiative fluxes of changingthe regression parameter by +1 standard deviation from the mean (standard deviations of the fluxes included for comparison)

Region	Parameter	Fvis	Fir	Fnet
90.0S-67.5S	T1000	0.000E+00	1.570E+01	-1.570E+01
	Xcld	0.000E+00	-1.907E-01	1.907E-01
Standard	Deviations:	0.000E+00	2.503E+01	
67.5S-45.0S	T1000	1.320E+01	8.026E+00	-2.123E+01
	Xcld	2.611E+00	-1.062E+01	8.010E+00
Standard	Deviations:	1.476E+01	2.138E+01	
45.0S-22.5S	T1000	2.614E+00	1.257E+01	-1.518E+01
	Xcld	1.201E+01	-2.285E+01	1.084E+01
Standard	Deviations:	1.853E+01	2.775E+01	
22.5S-0.0	T1000	3.250E+00	-1.026E+01	7.012E+00
	Xcld	1.777E+01	-1.849E+01	7.128E-01
Standard	Deviations:	2.591E+01	2.513E+01	
0.0-22.5N	T1000	-1.790E+00	-5.107E+00	6.897E+00
	Xcld	1.676E+01	-2.733E+01	1.058E+01
Standard	Deviations:	4.186E+01	4.365E+01	
22.5N-45.0N	T1000	-1.050E+01	1.348E+01	-2.983E+00
	Xcld	2.152E+01	-3.069E+01	9.169E+00
Standard	Deviations:	3.793E+01	3.833E+01	
45.0N-67.5N	T1000	-3.806E+01	1.148E+01	2.658E+01
	Xcld	4.278E+01	-1.670E+01	-2.608E+01
Standard	Deviations:	5.863E+01	2.290E+01	
67.5N-90.0N	T1000	-2.277E+01	2.633E+00	2.014E+01
	Xcld	2.266E+01	-6.910E+00	-1.575E+01
Standard	Deviations:	4.099E+01	1.071E+01	
Whole Earth	T1000	6.793E+00	2.778E+01	-3.457E+01
	Xcld	2.416E+01	-2.258E+01	-1.581E+00
Standard	Deviations:	6.732E+01	4.324E+01	